Journal of Materials Chemistry A

PAPER

Cite this: J. Mater. Chem. A, 2019, 7, 19961

Rationalizing the interphase stability of Li|doped-$Li_7La_3Zr_2O_{12}$ *via* automated reaction screening and machine learning†

Bo Liu,[ab] Jiong Yang,*[a] Hongliang Yang,[bc] Caichao Ye,[b] Yuanqing Mao,[b] Jiping Wang,[b] Siqi Shi,[a] Jihui Yang*[d] and Wenqing Zhang*[b]

Lithium metal batteries are a promising candidate for future high-energy-density energy storage. However, dendrite growth and the high reactivity of the Li metal anode result in low cycling efficiency and severe safety concerns. Here, we present a strategy to stabilize the lithium metal anode through cation doping in $Li_7La_3Zr_2O_{12}$ (LLZOM, M = dopant). High-throughput automated reaction screening together with a machine learning approach are developed to evaluate possible reactions and the thermodynamic stability of the Li|LLZOM interfaces under various chemical conditions. It is discovered that some dopants, such as M = Sc^{3+} (doping on Zr site), Ce^{3+} (La or Zr), Ac^{3+} (La), Y^{3+} (La or Zr), Tm^{3+} (La or Zr), Er^{3+} (La or Zr), Ho^{3+} (La or Zr), Dy^{3+} (La or Zr), Nd^{3+} (La or Zr), Tb^{3+} (La or Zr), Pr^{3+} (La), Pm^{3+} (La or Zr), Sm^{3+} (La or Zr), Gd^{3+} (La or Zr), Lu^{3+} (La), Ce^{4+} (Zr), Th^{4+} (Zr), and Pa^{5+} (Zr), exhibit thermodynamic stability against Li; while others, M = Ca^{2+} (La or Zr), Yb^{3+} (La), Br^{3+} (Li), Te^{4+} (Zr), Se^{4+} (Zr), S^{4+} (Zr), Hf^{4+} (Zr), Cl^{5+} (Zr), and I^{5+} (Zr), may lead to the spontaneous formation of a stable, passivating solid electrolyte interphase (SEI) layer on the Li metal, and alleviate dendritic lithium growth. From the machine learning approach, the formation energy of oxides M_xO_y emerges as the most crucial feature dominating the route of interface reactions, implying that the M–O bond strength governs the interface stability of the cation-doped LLZOM. The machine learning model then predicts 18 unexplored LLZOM systems, which are all validated in subsequent calculations. Our work offers practical insights for experimentalists into the selection of appropriate dopants in LLZO to stabilize Li metal anodes in solid-state batteries.

Received 23rd June 2019
Accepted 5th August 2019

DOI: 10.1039/c9ta06748e

rsc.li/materials-a

Introduction

Lithium (Li) metal is an ideal anode material for next-generation high-energy- and high-power-density batteries owing to its extremely high theoretical specific capacity (3860 mA h g^{-1}), low density (0.59 g cm^{-3} at room temperature), and the lowest negative electrochemical potential (−3.040 V *vs.* H/H^+).[1–3] Enabling Li metal anode has been regarded as the "Holy Grail" and is confronted by many challenges. Li dendrite formation and propagation, and Li anode pulverization in liquid electrolytes cause poor cycling performance, low coulombic efficiency, and severe safety concerns during battery cycling, which have hampered the practical applications of the Li metal anode over the past decades.[4,5] Solid-state electrolytes (SSEs) are a potential solution to these issues inherent to Li metal. Ideal SSE materials should possess high Li^+ conductivity (*e.g.*, >10^{-4} S cm^{-1} at room temperature), be electrically insulating, have a wide electrochemical window (*e.g.*, >6 V *vs.* Li^+/Li), possess stability against both electrodes and moisture, *etc.*[6] One major challenge in developing solid-state batteries stems from the lack of understanding of electrode–SSEs interfacial stability, specifically the Li metal–SSEs interface.[7,8] To prevent the reduction of Li metal, SSEs that are thermodynamically stable or that form stable passivation layers against Li metal are needed. The state-of-the-art SSE materials, including sulfides ($Li_{10}GeP_2S_{12}$ (ref. 9) and $Li_7P_3S_{11}$ (ref. 10)), oxynitrides (LiPON[11]), perovskite ($Li_{0.33}La_{0.56}TiO_3$ (ref. 12)), and NASICON-type ($Li_{1.3}Al_{0.3}Ti_{1.7}(PO_4)_3$ (ref. 13) and $LiZr_2(PO_4)_3$ (ref. 14)), can be reduced to form a solid electrolyte interphase (SEI) layer at the interface once in contact with the Li metal anode. If the SEI layer is electrically insulating, it passivates the SSE materials against further Li reduction, which is critical to achieve good stability.[15] Among various SSE materials, the garnet-type $Li_7La_3Zr_2O_{12}$ (LLZO) has drawn much attention because of its high Li^+ conductivity at room

[a]*Materials Genome Institute, Shanghai University, Shanghai 200444, China*
[b]*Department of Physics, Shenzhen Institute for Quantum Science & Technology, Southern University of Science and Technology, Shenzhen, Guangdong 518055, China*
[c]*State Key Laboratory of High Performance Ceramics and Superfine Microstructure, Shanghai Institute of Ceramics, Chinese Academy of Sciences, Shanghai 200050, China*
[d]*Department of Materials Science and Engineering, University of Washington, Seattle, WA 98195, USA. E-mail: jiongy@t.shu.edu.cn; zhangwq@sustc.edu.cn; jihuiy@uw.edu*

† Electronic supplementary information (ESI) available. See DOI: 10.1039/c9ta06748e

temperature (10^{-3} to 10^{-4} S cm^{-1}) and reasonable electrochemical stability against Li metal.[16–19]

It has been reported that cation doping in cubic LLZO, such as Nb^{5+}, Ta^{5+}, W^{6+}, or Mo^{6+} substituting for Zr^{4+},[20–23] as well as Al^{3+} or Ga^{3+} for the Li sublattice,[24,25] affects the cubic phase stability and increases the ionic conductivity. It was worth noting that the thermodynamic stability of the Li|LLZO interface is also affected by the doped cations. Nemori *et al.*[26] and Kim *et al.*[27] reported that Ta^{5+}-doped LLZO samples are stable in contact with Li, whereas those with Nb^{5+} are not. Ma *et al.*[28] investigated the reactions at the Li|cubic-$Li_{7-3x}Al_x$-$La_3Zr_2O_{12}$ (c-LLZO) interface, which forms a tetragonal-like LLZO interphase with 6 nm thickness, possibly inhibiting further chemical reactions. D. Rettenwander *et al.*[29] reported that $Li_{6.4}Fe_{0.2}La_3Zr_2O_{12}$, even with a high total conductivity of 1.1 mS cm^{-1} at room temperature, is not stable against Li metal and forms a thick tetragonal LLZO interlayer, causing high interfacial resistance. Nakayama *et al.*[18] used density functional theory (DFT) to investigate the electrochemical stability of different garnets with the composition Li_xLa_3-M_2O_{12} ($x = 5$ or 7; M = Ti, Zr, Nb, Ta, Sb, Bi) against Li metal and found that the electrochemical stability is strongly dependent on the effective charge states of the M cations. Moreover, a surface-science-based approach was used to successfully identify the reduction of different dopant species (Nb, Ta, and Al) in LLZO samples by Li metal, suggesting that dopants do indeed play a critical role in determining the reactivity of the Li|LLZO interface.[30,31] This leads to the hypothesis that the thermodynamic stability against Li metal of LLZO can be regulated by cation doping, which needs further validation.

So far, there has not been any systematic study on whether the cation doping of LLZO (labeled as LLZOM) improves its stability against Li metal. Owing to the lack of knowledge on the stability and composition-dependent reactions of LLZOM in contact with Li metal, prior studies on screening for appropriate dopants are mostly based on the trial-and-error approach. A predictive model for the thermodynamic stability of cation-doped LLZOM against Li metal is necessary. The present study is motivated by two fundamental questions. First, which cation dopant in LLZO is beneficial to the thermodynamic stability against Li metal? Second, what factors dominate the stability of Li|LLZOM interfaces?

In this paper, by using a first-principles approach based on a large-scale materials database, we build an automated route to screen all possible reactions corresponding to LLZOM in contact with varying amounts of Li, and to calculate the reaction energies ($\Delta G_{\mathrm{LLZOM-Li}}$) for the formation of the lowest-energy phases. We also obtain a machine learning model for classifying Li|LLZOM interfaces as thermodynamically stable or unstable with high accuracy. Our results reveal that the thermodynamic stability of LLZOM against Li metal can be improved when the dopant–oxygen bond in LLZOM is strong. By applying our machine learning model, 18 unexplored dopants M in LLZOM systems against Li metal are predicted and further validated in our automated calculations.

Methods

Formation energy calculations

In general, the formation energy for a compound is given by[32]

$$\Delta H_{\mathrm{f}} = E_{\mathrm{tot}} - \sum_i \mu_i x_i, \quad (1)$$

where E_{tot} is the DFT total energy of the compound, μ_i is the chemical potential of element i, and x_i is quantity of element i in the compound, respectively. As suggested by ref. 32, the DFT total energy of the elemental substance can be used as the chemical potential of each species. Strictly speaking, the computed formation energy is valid only for 0 K.

Phase stability calculations

The energy above the convex hull (E_{hull}) of each LLZOM compound was evaluated using pymatgen based on the DFT energies.[33] Stable compounds have an E_{hull} value of 0 eV per atom, and higher values indicate increasing metastability.

First-principles calculations

Density functional theory (DFT) calculations were performed within the generalized gradient approximation (GGA) with the Perdew, Burke and Ernzerhof (PBE) exchange–correlation functional,[34] using a plane wave basis set and the projector augmented wave (PAW) method[35] as implemented in the Vienna *Ab initio* Simulation Package (VASP) code.[36] Energy cutoff for the plane waves was set to be 520 eV. The convergence thresholds for self-consistency and forces were 10^{-5} eV and 10^{-2} eV Å^{-1}, respectively. The DFT+U was used to accurately describe the transition metal (Co, Cr, Fe, Mn, Mo, Ni, V, and W) for the strong correlation of d-electrons, and the U values were chosen with reference to the Materials Project (MP) database.[33] The energy correction for anions, transition metals, and gas/liquid phase was included in the MP database.[33] For pristine LLZO cells, we used an eight formula units conventional supercell, with cubic symmetry group $Ia\bar{3}d$. Li was distributed on the partially occupied 24d and 96h sites by using an electrostatic energy criterion that excluded occupation of electrostatically unfavorable first nearest-neighbor sites.[37] Before calculating the properties of doped LLZO, we compared the total energies of several pristine LLZO cells containing different distributions of Li ions across the available Li sites. The structure having the lowest total energy from this set of candidates was adopted for subsequent calculations.

Machine learning method

Support vector machine (SVM) classification. For the SVM classification problem, each instance of our data is described by an n-dimensional feature vector $\vec{x} = (f_1, f_2, f_3, \ldots, f_n)$ and a target label y. The label has a value of +1, say, for thermodynamically stable, and −1, for unstable. An SVM aims to find a function that for any given $\vec{x}$ has a value of ±1. Ideally, it is desired to generate a decision boundary in the space of features that maximizes the distance (also known as margin) of the closest instance of either class from it. Instances are defined as points

in the hyperspace of features that lie on one side or the other of this hypersurface. If we represent our input data by the set of label distances $\{(\vec{x}_i, y_i)\}$, then a soft margin support vector classifier determines the hypersurface in the space of features by solving

$$\alpha_1, \ldots, \alpha_n = \text{argmin} - \frac{1}{2}\sum_{i=1}^{m}\sum_{j=1}^{m}\alpha_i\alpha_j\kappa(\vec{x}_i, \vec{x}_j) + \sum_{i=1}^{m}\alpha_i, \quad (2)$$

subject to the following constraints

$$0 \le \alpha_i \le C \text{ and } \sum_{i=1}^{m}\alpha_i y_i = 0. \quad (3)$$

The kernel $\kappa(\vec{x}_i,\vec{x}_j)$ has linear kernels, polynomial kernels, or Gaussian kernels (radial *basis* function kernels, RBFs). In this work, however, after testing a number of kernels for their classification accuracies, we chose to go forward with a Gaussian kernel, defined as

$$\kappa(\vec{x}_i,\vec{x}_j) = \exp(-\gamma|\vec{x}_i - \vec{x}_j|^2). \quad (4)$$

Kernel ridge regression (KRR). Within the KRR model, the reaction energy of a system in the test set is given by a sum of a weighted Laplacian over the entire training set. As a part of the model training process, the learning is performed by minimizing the expression

$$\sum_{i=1}^{N}\left({G_{\text{KRR}}}^i - {G_{\text{DFT}}}^i\right)^2 + \lambda\sum_{i=1}^{N}{\omega_i}^2, \quad (5)$$

with ${G_{\text{KRR}}}^i$ being the KRR estimated reaction energy value, ${G_{\text{DFT}}}^i$ the DFT value, and λ a regularization parameter. The explicit solution to this minimization problem is $\omega = (k + \lambda I)^{-1}G_{\text{DFT}}$,

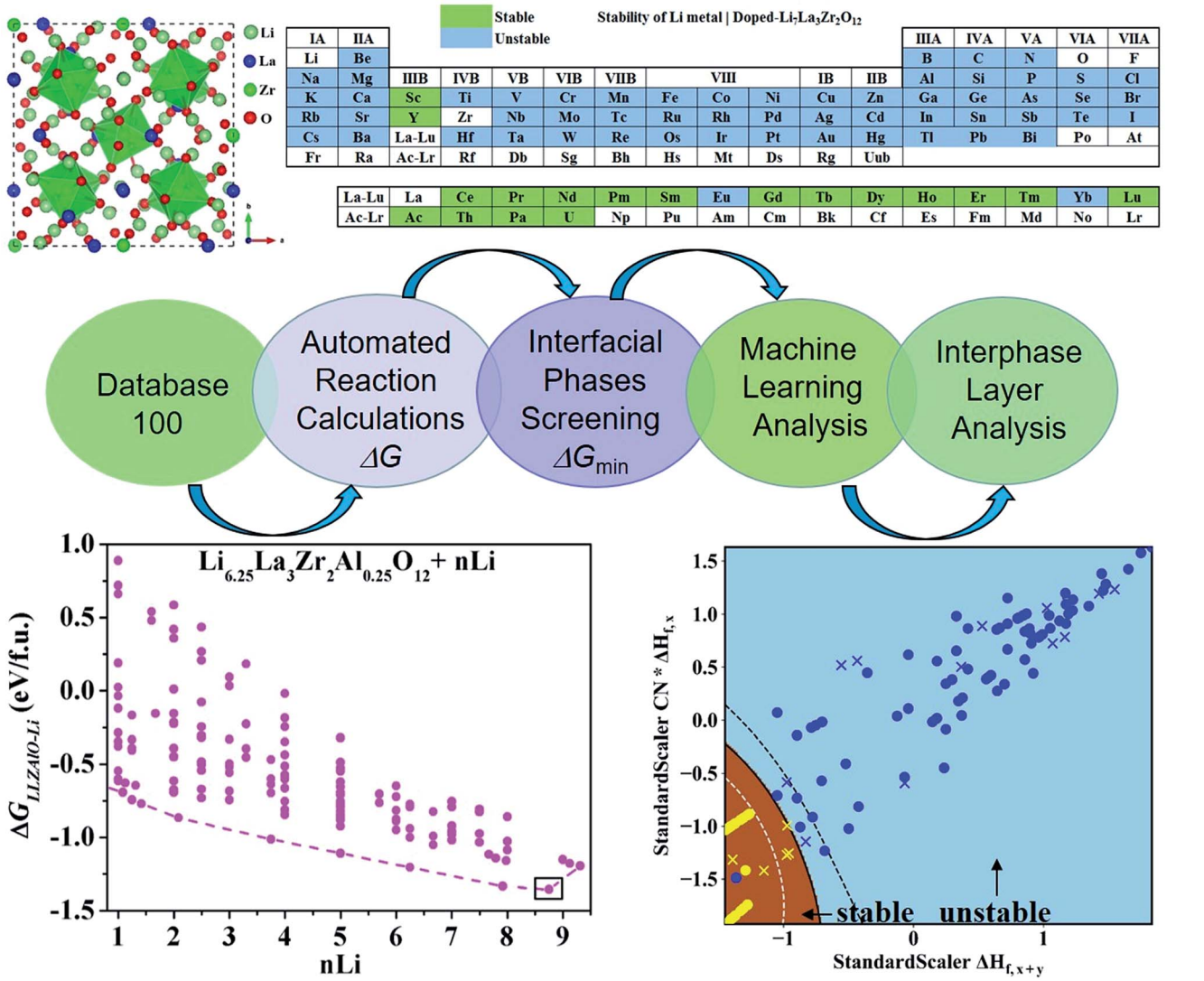

Fig. 1 The workflow of the automated interface reaction screening process and machine learning to efficiently search for cation-doped LLZO thermodynamically stable against Li metal used in LLZO-based all-solid batteries. The atomic structure, automated interface reaction screening, dopant screening, and interface stability machine learning classification results are presented.

where I is the identity matrix, and the kernel $\kappa(\vec{x}_i,\vec{x}_j)$ has linear kernels, polynomial kernels, Gaussian kernels (RBFs), or Laplacian kernels. In this work, however, after testing a number of kernels for their classification accuracies, we chose to go forward with a Laplacian kernel, defined as

$$K(\vec{x}_i,\vec{x}_j) = \exp\left(-\frac{1}{\sigma}|\vec{x}_i - \vec{x}_j|\right). \quad (6)$$

The parameters λ, σ are determined in an inner loop of five-fold cross-validation using a logarithmically scaled fine grid.

The coefficient of determination (R^2), employed to evaluate the model accuracy, is defined as

$$R^2 = 1 - \frac{\sum_i \left(y_i^{\text{true}} - y_i^{\text{pred}}\right)^2}{\sum_i \left(y_i^{\text{true}} - y_i^{-\text{true}}\right)^2}, \quad (7)$$

where y is the reaction energy value. The closer to 1 is the value of R^2, the better the fit of predicted values to the regression line. The mean squared error (MSE) represents the mean difference between the predicted values and the real values, defined as

$$\text{MSE} = \frac{1}{N}\sum_i^N |y_i^{\text{true}} - y_i^{\text{pred}}|. \quad (8)$$

Results and discussion

Automated reaction screening for possible interphases

To find the optimal cation doping in LLZO that can be stable against Li metal, we construct a screening workflow as illustrated in Fig. 1. First, a database containing the identities and formation energies of all of the relevant material phases, including the LLZOM phase and the product phases, is created, corresponding to more than 100 LLZOM structures which cover the Li-site, La-site, and Zr-site doping. For all calculations, we employ similar parameters, *e.g.*, the cutoff energy of plane waves, convergence criterion, *etc.*, in order to make all data comparable. The phase stability of the single phase LLZOM can be estimated by determining its E_{hull} value in the relevant multicomponent phase diagram. As shown in Fig. S1b,† each LLZOM has relatively small energy above the hull, suggesting that it has good phase stability. For each LLZOM reaction with Li metal, all possible product phases, including ternary compounds (Li–O–Zr, Li–O–M, La–Zr–O, La–M–O), binary compounds (Li–O, Zr–O, La–O, M–O, Zr–M), and simple substances (Zr, M) are considered. The structures and formation energies (ΔH_f) of the product phases are taken from the Materials Project (MP) database.[33] We compare the corresponding ΔH_f^{DFT} (ref. 33) and ΔH_f^{exp} (ref. 38 and 39) values of some product phases in Fig. S2.† The difference between the ΔH_f^{DFT} and ΔH_f^{exp} is relatively small, which implies DFT calculations can provide an acceptable level of accuracy in formation energy of product phases. Nevertheless, the reactant LLZOM has no matching entry with formation energies in MP; instead, a convex hull energy of LLZOM is used for reaction energy calculation. Herein, the formation energies of the LLZOM are calculated by DFT directly, which can increase the accuracy of the calculations for Li|LLZOM reactions. The possible reaction equations of LLZOM in contact with Li metal are constructed by an automatic reaction balance procedure. The high-throughput calculation framework used here relies on the availability of accurate formation energies to calculate the reaction energies of the Li|LLZOM interfaces, once the database is compiled.

From the large amount of calculated reaction energies data, the reactions with the lowest reaction energies are selected to be the most possible interphase reactions corresponding to the equilibrium product phases. This is a fully automated prediction of the product phases with different reactants. As a result, only the reaction-forming phase with the lowest reaction energy is adopted for further interface stability evaluations. The final thermodynamic stability of a specific Li|LLZOM interface is determined by whether the two materials have an exothermic reaction to form other phases. We calculate the reaction energies of LLZOM with metallic Li by reduction, according to the following equations

$$n\text{Li} + \text{LLZOM} \rightarrow \text{product phases}, \quad (9)$$

$$\Delta G_{\text{LLZOM–Li}} = E\,[\text{product phases}] - E\,[\text{LLZOM}] - nE\,[\text{Li}], \quad (10)$$

where the reaction energy $\Delta G_{\text{LLZOM–Li}}$ is the thermodynamic driving force for reactions between the LLZOM and Li, E [product phases] represents the formation energies of the product phases, and E [LLZOM] and E [Li] are the formation energies of the LLZOM and metallic lithium, respectively. Based on the calculated $\Delta G_{\text{LLZOM–Li}}$, Li|LLZOM reactions can be classified into two categories: (i) $\Delta G_{\text{LLZOM–Li}} > 0$, LLZOM phase in contact with Li is thermodynamically stable, namely, LLZOM and Li do not react with each other to form other phases in reduction processes; (ii) $\Delta G_{\text{LLZOM–Li}} < 0$, LLZOM phase is thermodynamically unstable, reacting with Li to form an interphase layer with various phases. All data about the formation energies of the LLZOM, reaction energies and product phases between Li metal and LLZOM compounds can be found in Table S1.† We further extract the reduction behavior of different doped systems and analyze the determining factors of cation doping on the stability of LLZO against Li metal by a machine learning approach. The formation energy of oxides M_xO_y, together with other feature factors, governs the stability of the Li|LLZOM interface. Furthermore, data analysis and visualization are performed to unravel the hidden trends. Given that a reasonable ionic conductivity is the precondition for solid electrolyte applications, we also perform bond-valence site energy (BVSE) calculations to evaluate the energy barriers of Li ion migration in each of the LLZOM compounds using our developed BVSE program,[40–42] and estimate the diffusion coefficient D by the equation $D = \nu a^2 \exp(-E_a/k_B T)$, as listed in Table S2.† The results show that high-valent dopants have an increasing trend in ionic conductivity, which is consistent with previous reports.[20–25]

As mentioned above, a successful workflow of the optimal dopant screening, including high-throughput interface reaction calculations and machine learning prediction, has been

demonstrated. For the high-throughput automated reaction calculations, using the Al-doped LLZO system as an example in Fig. 1 (bottom panels), only the reactions with the lowest reaction energies (bottom left panel), along the dashed line, represent the most likely decomposition path, *i.e.* the lithiation reaction of $Li_{7-x}La_3Zr_2Al_xO_{12}$ ($x = 0.25$). Fig. 2a shows that the reaction path starts with the product phases of La_2O_3, Li_5AlO_4, $Li_6Zr_2O_7$, and $ZrAl_3$; and eventually forms La_2O_3, Li_2O, Zr_4O, and Zr_3Al. The final product phases (La_2O_3, Li_2O, Zr_4O, and Zr_3Al) have a reaction energy of −1.244 eV per formula unit (f.u.). Fig. 2b shows the reaction energy for different dopant contents ($Li_{7-x}La_3Zr_2Al_xO_{12}$ with $x = 0.125$, 0.25). Overall, the reaction energy increases greatly with decreasing Al concentration, *e.g.*, as Al concentration decreases to 0.125, the reaction energy of the final product phases becomes −0.039 eV per formula unit. The results suggest that the thermodynamic stability of LLZOM against Li metal can be improved by controlling the dopant M contents. Higher M doping concentrations will cause instability of the Li|LLZOM interface (see ESI Fig. S3†).

M–O bond-strength-related interphase stability from data mining

In this section, we try to adopt the data mining technique to reveal the underlying mechanism of interfacial stability. Advanced machine learning methods become more and more important in the field of data mining as they have the potential to solve many complex problems, including prediction of physical properties and crystal structures, and uncover the physical mechanisms using a large amount of data from either high-throughput computation or experiments.[43–49] The key steps of data mining for the thermodynamic stability analysis of the Li|LLZOM interfaces are the selection of features (or descriptors) and the choice of model for machine learning algorithms.

The site and valence state for possible Li-, La-, and Zr-site dopants in LLZO, after filtering with a defect energy cutoff of 2 eV, are computed by DFT following previous work.[50] By applying this filter, the dataset for machine learning can be expanded. The dataset for this study comprises 100 LLZOM compounds, mainly from our own DFT calculations. The reaction data, *i.e.*, the reaction equation and reaction energy for each LLZOM against Li metal, are analyzed using an automatic reaction screening process. The Li|LLZOM interface is labeled ±1, with label +1 for a thermodynamically stable phase and label −1 for a thermodynamically unstable one. Typically, features are properties of a material that can distinguish one compound from others.[46,49,51] In our study, since the doping elements are different in LLZOM, we consider many relevant properties of the doping element as the features. Fifteen features for each LLZOM compound are selected for the machine learning procedure. They are: (i) valence states (VS) of dopant element M; (ii) ionic radius (r_M^i) and atomic radius (r_M^c) of element M from Shannon's work,[52] adopting the values under the same coordination number (CN) in LLZOM; (iii) atomic mass (AM) of element M; (iv) Pauling electronegativity (χ_M) of element M; (v) first ionization energy ($1^{st}IE_M$) of element M; (vi) the formation energy per atom defined as $\Delta H_{f,x+y} = \Delta H_f/(x+y)$, where ΔH_f is the heat for formation of the formula M_xO_y, the experimental formation energies from the SGTE Solid SUBstance (SSUB) database[39] and the thermodynamic database at the Thermal Processing Technology Center at the Illinois Institute of Technology (IIT),[38] and calculation formation energies from the MP database (see Table S3†). The majority of the calculated ΔH_f values are consistent with the measured data within ±0.2 eV per atom, with a few exceptions. (vii) Oxygen coordination number (CN) of dopant element M in LLZO; (viii) product of coordination number CN with the formation energy of oxide M_xO_y per M atom ($CN \times \Delta H_{f,x}$), and product of coordination number CN with the formation energy of oxide M_xO_y per oxygen atom ($CN \times \Delta H_{f,y}$), where $\Delta H_{f,x} = \Delta H_f/x$ and $\Delta H_{f,y} = \Delta H_f/y$. The parameters $CN \times \Delta H_{f,x}$ and $CN \times \Delta H_{f,y}$ can be possibly viewed as the effective measurement of local interaction strength with dopant M in LLZO. (ix) Ratio of M ionic radius to O ionic radius, denoted as r_M^i/r_O^i; (x) electron configurations of s + p, d and f orbitals of dopant element M; and (xi) bond dissociation energies (BDE) of M–O from the *Handbook of Chemical Bond Energies* (see Table S4†).[53] The random forest classifier in scikit-learn package[54] is adopted to measure the importance of the features by calculating their weights. As shown in Fig. 3, the formation energy ($\Delta H_{f,x+y}$) plays the most

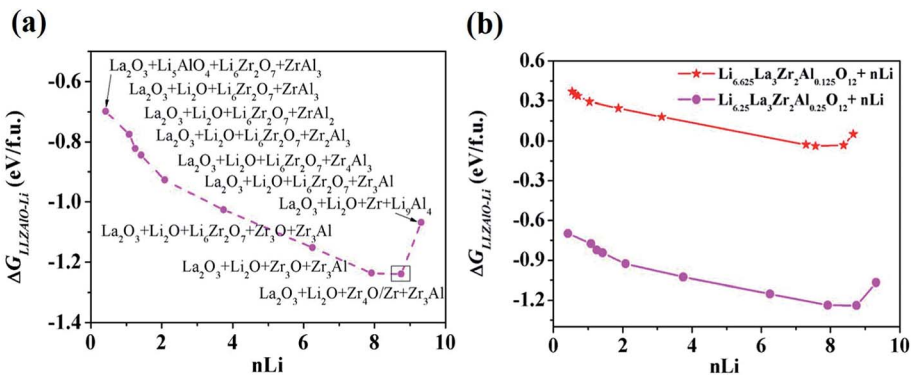

Fig. 2 The thermodynamic stability of LLZOAl when it reacts with Li. (a) The reaction paths and product phases along the dashed lines are marked, and the lowest reaction energy is marked with a square. (b) The reaction energy of the Li|LLZOAl interface *vs.* the doping concentration.

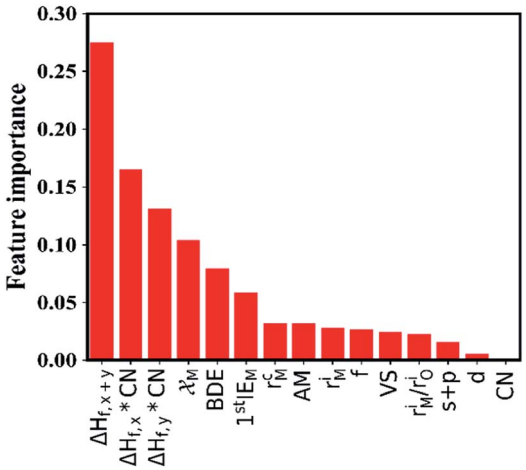

Fig. 3 The importance of the selected features. The 15 selected features are ranked using a random forest algorithm.

important role in determining the thermodynamic stability of LLZOM against Li, followed by the local interaction of M (CN × $\Delta H_{f,x}$, CN × $\Delta H_{f,y}$), the electronegativity (χ_M), and M–O bond dissociation energies (BDE). Pearson correlation coefficient (P) matrices are also calculated to identify the positive and negative correlations between pairs of features in Fig. S4.†

In our work, we adopt the machine learning technique in two different ways: (i) as a binary classification problem, where the machine should simple predict if the Li|LLZOM interface is thermodynamically stable (label 1) or not (label −1), and (ii) as a regression problem, where the machine predicts the reaction energy for the Li|LLZOM interface. In both situations, we adopt the machine learning model with best performance.[48] For example, five different classification algorithms, including logistic regression, support vector machine (SVM), decision tree, extra tree, and neural network, are adopted. Each classification algorithm is fitted using the training data with two, three, four, or even more features at a time. The SVM with Gaussian kernel algorithm is found to be the most effective model based on the five-fold cross-validation results, and the performance of the top five feature pairs is summarized in ESI Table S5.† The best feature pair is ($\Delta H_{f,x+y}$, CN × $\Delta H_{f,x}$), with both accuracy and F_1 score of 0.99(±0.02) for the test set. It is worth noting that all the five top-performing feature pairs contain $\Delta H_{f,x+y}$. Going beyond two features does not improve the model performance, so we use our best performing model (SVM) with two features for subsequent analyses and predictions.

The maps of the best feature pairs, *i.e.*, ($\Delta H_{f,x+y}$, CN × $\Delta H_{f,x}$) and ($\Delta H_{f,x+y}$, BDE), are shown in Fig. 4a and b, with yellow circles indicating thermodynamically stable ($\Delta G_{LLZOM-Li} > 0$) and blue ones unstable ($\Delta G_{LLZOM-Li} < 0$). Besides the 100 training data points, predictions were made for 18 unexplored compounds, labeled as crosses in Fig. 4. It is clear that compounds that are stable and unstable at Li|LLZOM interfaces are well separated by the black solid lines, which divide the ($\Delta H_{f,x+y}$, CN × $\Delta H_{f,x}$) and ($\Delta H_{f,x+y}$, BDE) maps into two regions with only a few exceptions. We observe that the 18 predicted data points (yellow crosses and blue crosses) are perfectly predicted by the training model, falling within the respective stable and unstable regions established by the training data. The ($\Delta H_{f,x+y}$, CN × $\Delta H_{f,y}$) and ($\Delta H_{f,x+y}$, χ_M) classification maps are also plotted in Fig. S5.† From the chemical bond point of view, since the selected features, such as ΔH_f and BDE, can be viewed as indicators of the M–O bond strength, based on our machine learning procedures it can be qualitatively concluded that the Li|LLZOM interface stability could be mainly measured by the local M–O chemical bond strength.

To quantitatively understand the Li|LLZOM interfacial thermodynamic stability, the reaction energies $\Delta G_{LLZOM-Li}$ and single

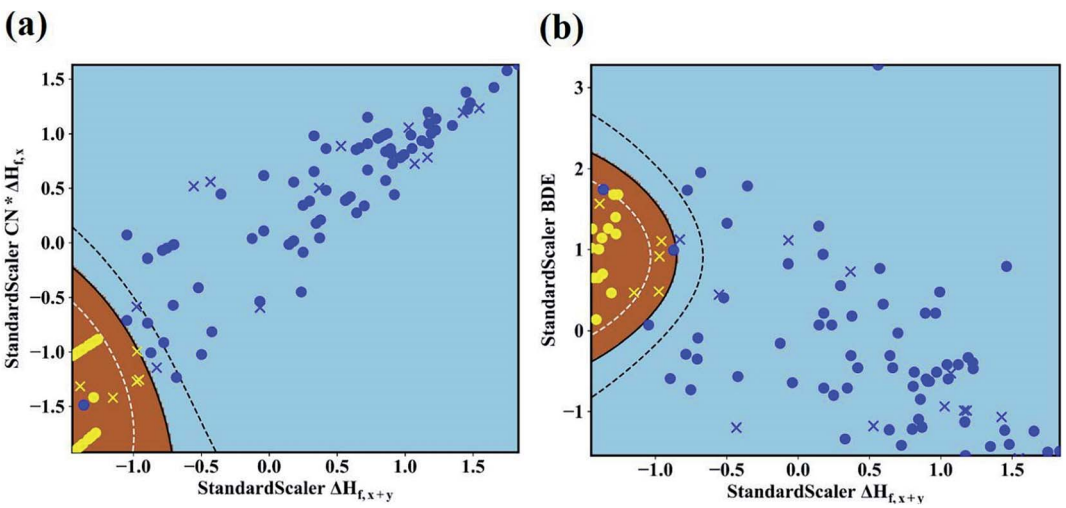

Fig. 4 Maps of (a) $\Delta H_{f,x+y}$ and CN × $\Delta H_{f,x}$, and (b) $\Delta H_{f,x+y}$ and M–O bond dissociation energy (BDE) feature pairs for 100 LLZOM compounds considered in our work. 18 unexplored data points are also predicted and plotted. Blue circles and yellow circles are the 100 training data points, and blue crosses and yellow crosses are the 18 predicted data points. The evaluation of classification performance for the SVM models involves feature pairs when both features are standard scalers. Brown and sky-blue areas represent thermodynamically stable and unstable regions, respectively.

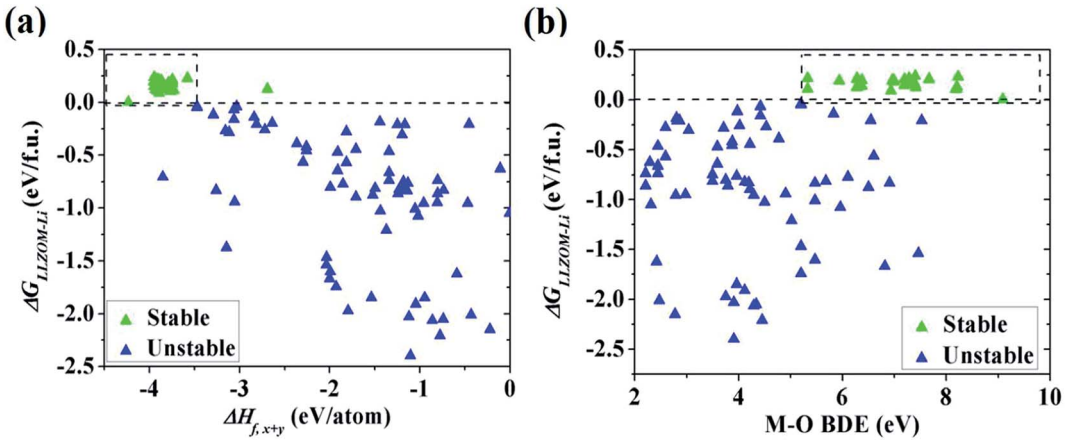

Fig. 5 The dependence of the reaction energy $\Delta G_{LLZOM-Li}$ of Li|LLZOM interface on (a) $\Delta H_{f,x+y}$ and (b) M–O bond dissociation energy. The dotted boxes represent the most appropriate range for each feature.

feature ($\Delta H_{f,x+y}$, BDE) relations are plotted in Fig. 5. We observe that oxides M_xO_y with larger negative formation energies ($|\Delta H_{f,x+y}|$ > 3.5 eV) give rise to more thermodynamically stable Li|LLZOM interfaces, and the M–O BDE directly reflects the local chemical bond strength of the initial LLZOM structure stability, shown in Fig. 5a and b, respectively. The greater the BDE, the more heat needs to be absorbed to disrupt the M–O bond in LLOZM during the chemical reactions. Similarly, it is clear that the majority of stable Li|LLZOM interfaces have a large negative CN × $\Delta H_{f,y}$ value, corresponding to the local chemical bond strength. In terms of the Pauling electronegativity χ_M, the appropriate range for Li|LLZOM interface stability is between 1.0 and 1.5 with only a few exceptions, as shown in ESI Fig. S6.† Therefore, we conclude that the thermodynamic stability of the Li|LLZOM interface relates to the stronger ionic bonding nature of M–O in LLZOM, which is in agreement with the report by Nakayama.[18]

In order to quantitatively obtain a prediction model for reaction energy ΔG, the KRR algorithm (with the best performance among five algorithms, see Table S8†) was employed. The model is based on the training data (80% of the full dataset), and is used to evaluate the test data. A plot of 100 LLZOM ΔG values predicted using KRR *versus* the DFT calculated values is presented in Fig. 6. The results clearly show good agreement between the DFT values and KRR predictions, with the R^2 and MSE of the test data as 0.92 and 0.04, respectively. Then, the trained KRR model is applied to the unexplored 18 LLZOM to predict their ΔG values, and the prediction results are listed in Table S6.† We notice that the predicted 18 ΔG values are in excellent correlation with the relevant feature statistics ($|\Delta H_{f,x+y}|$ > 3.5 eV; 1.0 < χ_M < 1.5). More importantly, the reaction energies of the 18 LLZOM systems are calculated by the automated reaction calculations, confirming the prediction model. Therefore, combining machine learning technology and high-throughput automated reaction calculations, we have developed an extremely fast target-driven method to predict the reaction energies for the Li|LLZOM interface systems. This workflow can be readily applied to other solid electrolyte materials.

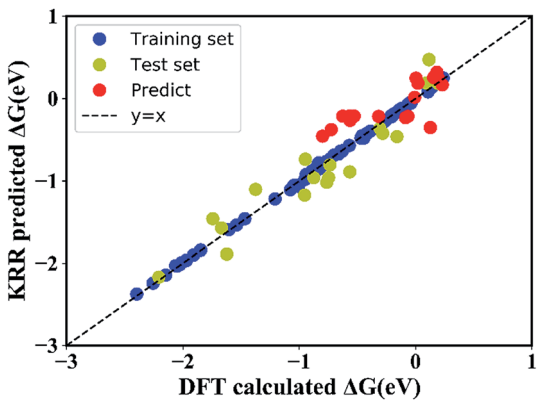

Fig. 6 DFT calculated reaction energies (ΔG) compared with the predicted reaction energies using a kernel ridge regression model. The model is trained on a randomly selected 80% training set from the 100 LLZOM database using the 15 features. The coefficient of determination (R^2) and mean squared error (MSE) are computed to estimate the prediction errors. The training and test points are show in blue and green, respectively. The perfect correlation line is included for reference as a black dashed line.

Beneficial effects of the interphase layer

Based on the automated reaction screening of the interfacial phases, an LLZOM that is unstable against Li metal would generate an interphase layer, similar to the formation of a solid electrolyte interphase (SEI) layer, as shown in Fig. 7. In fact, the interphase layer formed by the reactions also has the attribute of improving the stability of the interface, depending on the electrical conductivity of the product phases.[55] If the product phases are electrically insulating, they will form a passivated interface layer that promotes interfacial contacts and reduces the interfacial impedance.[56,57] In addition, the passivating interphase layer can prevent LLZOM from further reaction and suppress Li dendrite growth during cycling.[15,58] For example, some elements, M = Ca^{2+} (La or Zr), Yb^{3+} (La), Br^{3+} (Li), Te^{4+} (Zr), Se^{4+} (Zr), S^{4+} (Zr), Hf^{4+} (Zr), Cl^{5+} (Zr), and I^{5+} (Zr), when in equilibrium with Li metal, typically decompose into products

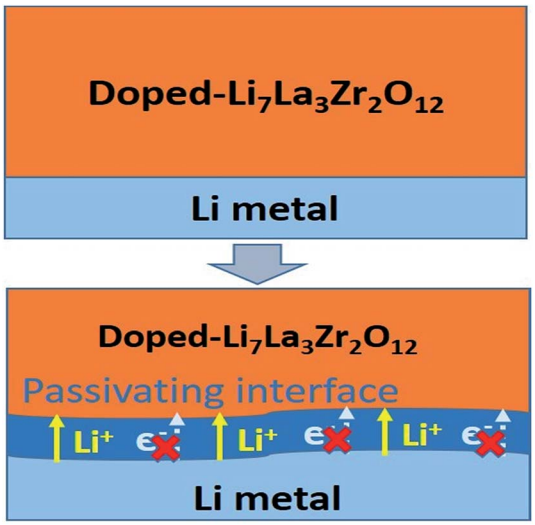

Fig. 7 Improvement of Li|LLZOM (M = dopants) interfacial stability *via* the formation of a passivating interface layer.

that are electrically insulating with bandgaps >2.0 eV (bandgap data from MP,[33] see Table S7†), *e.g.*, CaO, YbO, LiBr, La_2TeO_2, La_2SeO_2, La_2SO_2, $Li_6Hf_2O_7$, LiCl, and LaIO. For LLZOs with other dopants, the undesired high electrical conductivities of the interphase layers may cause continuous decomposition of the LLZOM materials, and a passivating interphase cannot be achieved at the interface.[59] In previous work, the non-passivating behavior of the interphase was confirmed, the interphase layers and the resistance increasing markedly in a short period of time.[9] Therefore, the electrical conductivity of the interphase layer is also a crucial factor in determining the interfacial stability of LLZOM against Li metal anode.

Conclusions

In this work, we have developed a high-throughput automated reaction screening and machine learning approach to evaluate possible reactions and the thermodynamic stability of Li|LLZOM interfaces under various chemical conditions. Our calculations reveal that LLZOM stability against Li metal is governed by the dopants. We discover that M = Sc^{3+} (Zr), Ce^{3+} (Zr or La), Ac^{3+} (La), Y^{3+} (La or Zr), Tm^{3+} (La or Zr), Er^{3+} (La or Zr), Ho^{3+} (La or Zr), Dy^{3+} (La or Zr), Nd^{3+} (La or Zr), Tb^{3+} (La or Zr), Pr^{3+} (La), Pm^{3+} (La or Zr), Sm^{3+} (La or Zr), Gd^{3+} (La or Zr), Lu^{3+} (La), Ce^{4+} (Zr), Th^{4+} (Zr), Pa^{5+} (Zr), Ca^{2+} (La or Zr), Yb^{3+} (La), Br^{3+} (Li), Te^{4+} (Zr), Se^{4+} (Zr), S^{4+} (Zr), Hf^{4+} (Zr), Cl^{5+} (Zr), and I^{5+} (Zr) exhibit stability against Li metal, either because the interface is thermodynamically stable or as a result of stable passivation. However, LLZOMs with other dopant cations are likely reduced by Li metal, while passivating interphases cannot be achieved at the interface. On the basis of a large amount of data, we have attempted to find the underlying physical mechanisms of the thermodynamic stability of Li|LLZOM interfaces by employing a machine learning technique. Based on our analysis, the stability of the Li|LLZOM interface is determined by the M–O chemical bond strength. Our results provide a guiding principle for selecting cation doping in LLZO to provide stability against Li metal, and show the potential for the fast screening of new LLZOM materials by the machine learning approach.

Conflicts of interest

The authors declare that there are no conflicts of interest.

Acknowledgements

This work was supported by the National Key Research and Development Program of China (No. 2017YFB0701600), the Natural Science Foundation of China (Grant Nos. 51572167, 51632005, 51622207, and U1630134), and the 111 project D16002. Jihui Yang acknowledges support from the Inamori Foundation. W. Q. Zhang acknowledges the support Program of Shanghai Subject Chief Scientist (16XD1401100), Guangdong Innovation Team Project (Grant No. 2017ZT07C062), and the Shenzhen Pengcheng-Scholarship Program.

References

1 W. Xu, J. Wang, F. Ding, X. Chen, E. Nasybulin, Y. Zhang and J.-G. Zhang, *Energy Environ. Sci.*, 2014, **7**, 513–537.
2 D. Lin, Y. Liu and Y. Cui, *Nat. Nanotechnol.*, 2017, **12**, 194.
3 B. Liu, J.-G. Zhang and W. Xu, *Joule*, 2018, **2**, 833–845.
4 X.-B. Cheng, R. Zhang, C.-Z. Zhao and Q. Zhang, *Chem. Rev.*, 2017, **117**, 10403–10473.
5 X. Q. Zhang, X. B. Cheng and Q. Zhang, *Adv. Mater. Interfaces*, 2018, **5**, 1701097.
6 H. Duan, H. Zheng, Y. Zhou, B. Xu and H. Liu, *Solid State Ionics*, 2018, **318**, 45–53.
7 F. Han, J. Yue, C. Chen, N. Zhao, X. Fan, Z. Ma, T. Gao, F. Wang, X. Guo and C. Wang, *Joule*, 2018, **2**, 497–508.
8 A. Wang, S. Kadam, H. Li, S. Shi and Y. Qi, *npj Comput. Mater.*, 2018, **4**, 15.
9 S. Wenzel, S. Randau, T. Leichtweiß, D. A. Weber, J. Sann, W. G. Zeier and J. Janek, *Chem. Mater.*, 2016, **28**, 2400–2407.
10 S. Wenzel, D. A. Weber, T. Leichtweiss, M. R. Busche, J. Sann and J. Janek, *Solid State Ionics*, 2016, **286**, 24–33.
11 A. Schwöbel, R. Hausbrand and W. Jaegermann, *Solid State Ionics*, 2015, **273**, 51–54.
12 S. Stramare, V. Thangadurai and W. Weppner, *Chem. Mater.*, 2003, **15**, 3974–3990.
13 H. Aono, E. Sugimoto, Y. Sadaoka, N. Imanaka and G. y. Adachi, *J. Electrochem. Soc.*, 1990, **137**, 1023–1027.
14 Y. Li, W. Zhou, X. Chen, X. Lü, Z. Cui, S. Xin, L. Xue, Q. Jia and J. B. Goodenough, *Proc. Natl. Acad. Sci. U. S. A.*, 2016, **113**, 13313–13317.
15 B. Wu, S. Wang, J. Lochala, D. Desrochers, B. Liu, W. Zhang, J. Yang and J. Xiao, *Energy Environ. Sci.*, 2018, **11**, 1803–1810.
16 M. Ramaswamy, T. Venkataraman and W. Werner, *Angew. Chem., Int. Ed.*, 2007, **46**, 7778–7781.
17 M. Kotobuki, H. Munakata, K. Kanamura, Y. Sato and T. Yoshida, *J. Electrochem. Soc.*, 2010, **157**, A1076–A1079.

18 M. Nakayama, M. Kotobuki, H. Munakata, M. Nogami and K. Kanamura, *Phys. Chem. Chem. Phys.*, 2012, **14**, 10008–10014.

19 T. Thompson, S. Yu, L. Williams, R. D. Schmidt, R. Garcia-Mendez, J. Wolfenstine, J. L. Allen, E. Kioupakis, D. J. Siegel and J. Sakamoto, *ACS Energy Lett.*, 2017, **2**, 462–468.

20 S. Ohta, T. Kobayashi and T. Asaoka, *J. Power Sources*, 2011, **196**, 3342–3345.

21 H. Buschmann, S. Berendts, B. Mogwitz and J. Janek, *J. Power Sources*, 2012, **206**, 236–244.

22 P. Bottke, D. Rettenwander, W. Schmidt, G. Amthauer and M. Wilkening, *Chem. Mater.*, 2015, **27**, 6571–6582.

23 Y. Li, Z. Wang, Y. Cao, F. Du, C. Chen, Z. Cui and X. Guo, *Electrochim. Acta*, 2015, **180**, 37–42.

24 J. Wolfenstine, J. Ratchford, E. Rangasamy, J. Sakamoto and J. L. Allen, *Mater. Chem. Phys.*, 2012, **134**, 571–575.

25 D. Rettenwander, P. Blaha, R. Laskowski, K. Schwarz, P. Bottke, M. Wilkening, C. A. Geiger and G. Amthauer, *Chem. Mater.*, 2014, **26**, 2617–2623.

26 H. Nemori, Y. Matsuda, S. Mitsuoka, M. Matsui, O. Yamamoto, Y. Takeda and N. Imanishi, *Solid State Ionics*, 2015, **282**, 7–12.

27 Y. Kim, A. Yoo, R. D. Schmidt, A. Sharafi, H. Lee, J. Wolfenstine and J. Sakamoto, *Front. Energy Res.*, 2016, **4**, 1–7.

28 C. Ma, Y. Cheng, K. Yin, J. Luo, A. Sharafi, J. Sakamoto, J. Li, K. L. More, N. J. Dudney and M. Chi, *Nano Lett.*, 2016, **16**, 7030–7036.

29 D. Rettenwander, R. Wagner, A. Reyer, M. Bonta, L. Cheng, M. M. Doeff, A. Limbeck, M. Wilkening and G. Amthauer, *J. Phys. Chem. C*, 2018, **122**, 3780–3785.

30 J. G. Connell, Y. Zhu, P. Zapol, S. Tepavcevic, A. Sharafi, J. Sakamoto, L. A. Curtiss, D. D. Fong, J. W. Freeland and N. M. Markovic, *ACS Appl. Mater. Interfaces*, 2018, **10**, 17471–17479.

31 Y. Zhu, J. G. Connell, S. Tepavcevic, P. Zapol, R. Garcia-Mendez, N. J. Taylor, J. Sakamoto, B. J. Ingram, L. A. Curtiss, J. W. Freeland, D. D. Fong and N. M. Markovic, *Adv. Energy Mater.*, 2019, **9**, 1803440.

32 S. Kirklin, J. E. Saal, B. Meredig, A. Thompson, J. W. Doak, M. Aykol, S. Rühl and C. Wolverton, *npj Comput. Mater.*, 2015, **1**, 15010.

33 S. P. Ong, W. D. Richards, A. Jain, G. Hautier, M. Kocher, S. Cholia, D. Gunter, V. L. Chevrier, K. A. Persson and G. Ceder, *Comput. Mater. Sci.*, 2013, **68**, 314–319.

34 K. B. John, P. Perdew and M. Ernzerhof, *Phys. Rev. Lett.*, 1996, **77**, 3865–3868.

35 G. Kresse, *Phys. Rev. B*, 1999, **59**, 1758–1775.

36 G. Kresse, *Phys. Rev. B*, 1996, **54**, 11169–11186.

37 P. P. Ewald, *Ann. Phys.*, 1921, **369**, 253–287.

38 P. Nash, https://tptc.iit.edu/index.php/thermo-database, 2013.

39 L. f. T. Hüttenkunde and R.-W. T. H. Aachen, *Thermodynamic Properties of Inorganic Materials, Landolt-Börnstein, New Series*, 1999, vol. 19.

40 B. He and S. Shi, *Screening platform for solid electrolyte*, Shanghai University, 2018, https://www.bmaterials.cn.

41 R. Xiao, H. Li and L. Chen, *Sci. Rep.*, 2015, **5**, 14227.

42 L. Pan, L. Zhang, A. Ye, S. Chi, Z. Zou, B. He, L. Chen, Q. Zhao, D. Wang and S. Shi, *J. Materiomics*, 2019, DOI: 10.1016/j.jmat.2019.04.010.

43 G. Pilania, P. V. Balachandran, C. Kim and T. Lookman, *Front. Mater.*, 2016, **3**, 1–7.

44 S. Shi, J. Gao, Y. Liu, Y. Zhao, Q. Wu, W. Ju, C. Ouyang and R. Xiao, *Chin. Phys. B*, 2016, **25**(1), 018212.

45 Y. Liu, T. Zhao, W. Ju and S. Shi, *J. Materiomics*, 2017, **3**, 159–177.

46 J. Schmidt, J. Shi, P. Borlido, L. Chen, S. Botti and M. A. L. Marques, *Chem. Mater.*, 2017, **29**, 5090–5103.

47 Y. Wang, W. Zhang, L. Chen, S. Shi and J. Liu, *Sci. Technol. Adv. Mater.*, 2017, **18**, 134–146.

48 W. Li, R. Jacobs and D. Morgan, *Comput. Mater. Sci.*, 2018, **150**, 454–463.

49 S. Lu, Q. Zhou, Y. Ouyang, Y. Guo, Q. Li and J. Wang, *Nat. Commun.*, 2018, **9**, 3405.

50 L. J. Miara, W. D. Richards, Y. E. Wang and G. Ceder, *Chem. Mater.*, 2015, **27**, 4040–4047.

51 A. O. Oliynyk, E. Antono, T. D. Sparks, L. Ghadbeigi, M. W. Gaultois, B. Meredig and A. Mar, *Chem. Mater.*, 2016, **28**, 7324–7331.

52 R. Shannon, *Acta Crystallogr., Sect. A: Cryst. Phys., Diffr., Theor. Gen. Crystallogr.*, 1976, **32**, 751–767.

53 Y. R. Luo, *Comprehensive Handbook of Chemical Bond Energies*, CRC Press, Boca Raton, FL, 2007.

54 F. Pedregosa, G. Varoquaux, A. Gramfort, V. Michel, B. Thirion, O. Grisel, M. Blondel, P. Prettenhofer, R. Weiss, V. Dubourg, J. Vanderplas, A. Passos, D. Cournapeau, M. Brucher, M. Perrot and E. Duchesnay, *J. Mach. Learn. Res.*, 2011, **12**, 2825–2830.

55 Y. Shen, Y. Zhang, S. Han, J. Wang, Z. Peng and L. Chen, *Joule*, 2018, **2**, 1674–1689.

56 X. Han, Y. Gong, K. Fu, X. He, G. T. Hitz, J. Dai, A. Pearse, B. Liu, H. Wang, G. Rubloff, Y. Mo, V. Thangadurai, E. D. Wachsman and L. Hu, *Nat. Mater.*, 2016, **16**, 572.

57 K. Fu, Y. Gong, B. Liu, Y. Zhu, S. Xu, Y. Yao, W. Luo, C. Wang, S. D. Lacey, J. Dai, Y. Chen, Y. Mo, E. Wachsman and L. Hu, *Sci. Adv.*, 2017, **3**, e1601659.

58 Z. Zhang, L. Zhang, Y. Liu, H. Wang, C. Yu, H. Zeng, L.-m. Wang and B. Xu, *ChemSusChem*, 2018, **11**, 3774–3782.

59 Y. Z. Zhu, X. F. He and Y. F. Mo, *Adv. Sci.*, 2017, **4**, 1600517.

Electronic Supplementary Material (ESI) for Journal of Materials Chemistry A.

Supporting Information

Rationalize the interphase stability of Li|doped-$Li_7La_3Zr_2O_{12}$ via automated reaction screening and machine learning

Bo Liu[a,b], Jiong Yang[a,*], Hongliang Yang[b,c], Caichao Ye[b], Yuanqing Mao[b], Jiping Wang[b], Siqi Shi[a], Jihui Yang[d,*], and Wenqing Zhang[b,*]

[a]Materials Genome Institute, Shanghai University, Shanghai 200444, China

[b]Department of Physics and Shenzhen Institute for Quantum Science & Technology, Southern University of Science and Technology, Shenzhen, Guangdong 518055, China

[c]State Key Laboratory of High Performance Ceramics and Superfine Microstructure, Shanghai Institute of Ceramics, Chinese Academy of Sciences, Shanghai 200050, China

[d]Department of Materials Science and Engineering, University of Washington, Seattle, WA 98195, USA

Table S1. The complete computational results of lithiation reactions for LLZOM (M = dopants). The reaction energy ΔG is normalized to per formula-unit for the lithiation of LLZOM to form the phase equilibria with Li metal. The LLZOM compounds were thermodynamically stable against Li metal, which has a positive reaction energy value in complete lithiated process. The left side of the reaction energy column is our calculation result, and the right side is the result of MP[1] database.

System	Doped Site	Dopant	Oxidation state	Formation energy (eV/atom)	Li number	Reaction energy $\Delta G/\Delta G_{MP}$ (eV/atom)	Reaction products			
Li56La24Zr16O96				-3.128	6.667	-0.0224/-0.016	La2O3	Li2O	Zr3O	
					7.000	-0.0226/-0.016	La2O3	Li2O	Zr4O	
					8.000	-0.0216	La2O3	Li2O	Zr	
Li53La24Zr16AlO96	Li	Al	3	-3.195	0.542	0.0153	La2O3	Li2O	Li6Zr2O7	ZrAl3
					0.625	0.0143/-0.003	La2O3	Li2O	Li6Zr2O7	ZrAl2
					0.708	0.0138/-0.004	La2O3	Li2O	Li6Zr2O7	Zr2Al3
					1.042	0.0119/-0.005	La2O3	Li2O	Li6Zr2O7	Zr4Al3
					1.875	0.0096/-0.007	La2O3	Li2O	Li6Zr2O7	Zr3Al
					7.292	-0.0009/-0.014	La2O3	Li2O	Zr3O	Zr3Al
					7.563	-0.0012/-0.015	La2O3	Li2O	Zr4O	Zr3Al
					8.375	-0.0010	La2O3	Li2O	Zr	Zr3Al
					8.656	0.0016	La2O3	Li2O	Zr	Li9Al4
Li50La24Zr16Al2O96	Li	Al	3	-3.184	0.419	-0.0292	La2O3	Li5AlO4	Li6Zr2O7	ZrAl3
					1.083	-0.0315	La2O3	Li2O	Li6Zr2O7	ZrAl3
					1.250	-0.0332/-0.009	La2O3	Li2O	Li6Zr2O7	ZrAl2
					1.417	-0.0339/-0.010	La2O3	Li2O	Li6Zr2O7	Zr2Al3
					2.083	-0.0362/-0.013	La2O3	Li2O	Li6Zr2O7	Zr4Al3
					3.750	-0.0377/-0.016	La2O3	Li2O	Li6Zr2O7	Zr3Al
					7.917	-0.0394/-0.020	La2O3	Li2O	Zr3O	Zr3Al
					8.125	-0.0393/-0.020	La2O3	Li2O	Zr4O	Zr3Al
					8.750	-0.0384	La2O3	Li2O	Zr	Zr3Al
Li53La24Zr16GaO96	Li	Ga	3	-3.180	0.375	0.0042/-0.013	La2O3	Li2O	Li6Zr2O7	Ga
					0.411	0.0030/-0.015	La2O3	Li2O	Li6Zr2O7	Li2Ga7
					0.437	0.0023/-0.015	La2O3	Li2O	Li6Zr2O7	LaGa6
					0.500	0.0009/-0.017	La2O3	Li2O	Li6Zr2O7	LiGa
					0.542	0.0006	La2O3	Li2O	Li6Zr2O7	ZrGa3
					0.562	-0.0001/-0.018	La2O3	Li2O	Li6Zr2O7	LaGa2
					0.625	-0.0005	La2O3	Li2O	Li6Zr2O7	ZrGa2
					0.708	-0.0016/-0.019	La2O3	Li2O	Li6Zr2O7	Zr2Ga3
					0.875	-0.0031/-0.020	La2O3	Li2O	Li6Zr2O7	ZrGa
					1.125	-0.0040/-0.021	La2O3	Li2O	Li6Zr2O7	Zr3Ga2
					1.375	-0.0046/-0.021	La2O3	Li2O	Li6Zr2O7	Zr2Ga

					7.208	-0.0132/-0.027	La2O3	Li2O	Zr3O	Zr2Ga
					7.500	-0.0134/-0.027	La2O3	Li2O	Zr4O	Zr2Ga
					8.375	-0.0129	La2O3	Li2O	Zr	Zr2Ga
Li53La24Zr16BrO96	Li	Br	3	-3.144	0.500	-0.047/-0.060	La2O3	Li2O	Li6Zr2O7	LiBr
					7.167	-0.048/-0.058	La2O3	Li2O	Zr3O	LiBr
					7.500	-0.048/-0.057	La2O3	Li2O	Zr4O	LiBr
					8.500	-0.0461	La2O3	Li2O	Zr	LiBr
Li53La24Zr16BO96	Li	B	3	-3.190	0.625	0.0058/-0.012	La2O3	Li2O	Li6Zr2O7	ZrB2
					7.083	-0.0059/-0.019	La2O3	Li2O	Zr3O	ZrB2
					7.406	-0.0063/-0.020	La2O3	Li2O	Zr4O	ZrB2
					8.375	-0.0059	La2O3	Li2O	Zr	ZrB2
Li54La24Zr16ZnO96	Li	Zn	2	-3.165	0.250	0.0058/-0.012	La2O3	Li2O	Li6Zr2O7	Zn
					0.279	0.0049/-0.013	La2O3	Li2O	Li6Zr2O7	LaZn13
					0.284	0.0048/-0.013	La2O3	Li2O	Li6Zr2O7	LaZn11
					0.294	0.0046/-0.013	La2O3	Li2O	Li6Zr2O7	La2Zn17
					0.375	0.0036/-0.014	La2O3	Li2O	Li6Zr2O7	LiZn
					0.417	0.0036	La2O3	Li2O	Li6Zr2O7	ZrZn3
					0.500	0.0031	La2O3	Li2O	Li6Zr2O7	ZrZn2
					0.750	0.0020/-0.016	La2O3	Li2O	Li6Zr2O7	ZrZn
					7.000	-0.0086/-0.022	La2O3	Li2O	Zr3O	ZrZn
					7.312	-0.0089/-0.023	La2O3	Li2O	Zr4O	ZrZn
					8.250	-0.0084	La2O3	Li2O	Zr	ZrZn
Li54La24Zr16CdO96	Li	Cd	2	-3.158	0.250	-0.0010/-0.018	La2O3	Li2O	Li6Zr2O7	Cd
					0.292	-0.0023/-0.019	La2O3	Li2O	Li6Zr2O7	LiCd3
					0.375	-0.0037/-0.020	La2O3	Li2O	Li6Zr2O7	LiCd
					0.625	-0.0047/-0.021	La2O3	Li2O	Li6Zr2O7	Li3Cd
					7.292	-0.0145/-0.027	La2O3	Li2O	Zr3O	Li3Cd
					7.625	-0.0147/-0.027	La2O3	Li2O	Zr4O	Li3Cd
					8.625	-0.0141	La2O3	Li2O	Zr	Li3Cd
Li53La24Zr16FeO96	Li	Fe	3	-3.164	0.375	-0.0115/-0.020	La2O3	Li2O	Li6Zr2O7	Fe
					0.625	-0.0140/-0.022	La2O3	Li2O	Li6Zr2O7	ZrFe2
					1.875	-0.0158/-0.024	La2O3	Li2O	Li6Zr2O7	Zr3Fe
					7.292	-0.0219/-0.028	La2O3	Li2O	Zr3O	Zr3Fe
					7.562	-0.0220/-0.028	La2O3	Li2O	Zr4O	Zr3Fe
					8.375	-0.0213	La2O3	Li2O	Zr	Zr3Fe
Li58La23Zr16KO96	La	K	1	-3.114	0.125	0.0057/-0.003	La2O3	Li2O	Li6Zr2O7	K
					6.792	-0.0063/-0.013	La2O3	Li2O	Zr3O	K
					7.125	-0.0066/-0.013	La2O3	Li2O	Zr4O	K
					8.125	-0.0062	La2O3	Li2O	Zr	K
Li58La23Zr16NaO96	La	Na	1	-3.115	0.125	0.0067/-0.003	La2O3	Li2O	Li6Zr2O7	Na
					6.792	-0.0055/-0.013	La2O3	Li2O	Zr3O	Na

					7.125	-0.0059/-0.013	La2O3	Li2O	Zr4O	Na
					8.125	-0.0055	La2O3	Li2O	Zr	Na
Li58La23Zr16RbO96	La	Rb	1	-3.114	0.125	0.0057/-0.005	La2O3	Li2O	Li6Zr2O7	Rb
					6.792	-0.0063/-0.014	La2O3	Li2O	Zr3O	Rb
					7.125	-0.0066/-0.015	La2O3	Li2O	Zr4O	Rb
					8.125	-0.0062	La2O3	Li2O	Zr	Rb
Li58La23Zr16CsO96	La	Cs	1	-3.110	0.125	0.0018/-0.005	La2O3	Li2O	Li6Zr2O7	Cs
					6.792	-0.0094/-0.015	La2O3	Li2O	Zr3O	Cs
					7.125	-0.0097/-0.015	La2O3	Li2O	Zr4O	Cs
					8.125	-0.0092	La2O3	Li2O	Zr	Cs
Li58La23Zr16AgO96	La	Ag	1	-3.100	0.125	-0.0082/-0.012	La2O3	Li2O	Li6Zr2O7	Ag
					0.167	-0.0091/-0.013	La2O3	Li2O	Li6Zr2O7	LiAg3
					0.250	-0.0104/-0.015	La2O3	Li2O	Li6Zr2O7	LiAg
					0.325	-0.0107/-0.015	La2O3	Li2O	Li6Zr2O7	Li8Ag5
					0.500	-0.0113/-0.015	La2O3	Li2O	Li6Zr2O7	Li3Ag
					1.125	-0.0111	La2O3	Li2O	Li6Zr2O7	Zr2Ag
					6.958	-0.0185	La2O3	Li2O	Zr3O	Zr2Ag
					7.167	-0.0196/-0.023	La2O3	Li2O	Zr3O	Li3Ag
					7.500	-0.0198/-0.023	La2O3	Li2O	Zr4O	Li3Ag
					8.500	-0.0190	La2O3	Li2O	Zr	Li3Ag
Li57La23Zr16BaO96	La	Ba	2	-3.133	0.250	0.0086/-0.001	La2O3	Li2O	Li6Zr2O7	Ba
					6.917	-0.0041/-0.011	La2O3	Li2O	Zr3O	Ba
					7.250	-0.0044/-0.012	La2O3	Li2O	Zr4O	Ba
					8.250	-0.0041	La2O3	Li2O	Zr	Ba
Li57La23Zr16CaO96	La	Ca	2	-3.136	0.250	0.0116	La2O3	Li2O	Li6Zr2O7	Ca
					6.667	-0.0034/-0.011	La2O3	Li2O	Zr3O	CaO
					7.000	-0.0038/-0.011	La2O3	Li2O	Zr4O	CaO
					8.000	-0.0034	La2O3	Li2O	Zr	CaO
Li57La23Zr16SrO96	La	Sr	2	-3.136	0.250	0.0116	La2O3	Li2O	Li6Zr2O7	Sr
					6.667	-0.0016/-0.011	La2O3	Li2O	Zr3O	SrO
					7.000	-0.0020/-0.011	La2O3	Li2O	Zr4O	SrO
					7.250	-0.0021/-0.011	La2O3	Li2O	Zr4O	Sr
					7.333	-0.0021/-0.011	La2O3	Li2O	Zr4O	Sr3Li2
					8.333	-0.0018	La2O3	Li2O	Zr	Sr3Li2
Li57La23Zr16PbO96	La	Pb	2	-3.115	0.250	-0.0092/-0.017	La2O3	Li2O	Li6Zr2O7	Pb
					0.375	-0.0120/-0.019	La2O3	Li2O	Li6Zr2O7	LiPb
					0.583	-0.0151/-0.022	La2O3	Li2O	Li6Zr2O7	Li8Pb3
					0.625	-0.0156/-0.023	La2O3	Li2O	Li6Zr2O7	Li3Pb
					0.687	-0.0162/-0.024	La2O3	Li2O	Li6Zr2O7	Li7Pb2
					0.781	-0.0166/-0.024	La2O3	Li2O	Li6Zr2O7	Li17Pb4
					7.448	-0.0238/-0.029	La2O3	Li2O	Zr3O	Li17Pb4

					7.781	-0.0239/-0.029	La2O3	Li2O	Zr4O	Li17Pb4
					8.781	-0.0230	La2O3	Li2O	Zr	Li17Pb4
Li57La23Zr16CdO96	La	Cd	2	-3.112	0.250	-0.0122/-0.018	La2O3	Li2O	Li6Zr2O7	Cd
					0.292	-0.0134/-0.019	La2O3	Li2O	Li6Zr2O7	LiCd3
					0.375	-0.0147/-0.020	La2O3	Li2O	Li6Zr2O7	LiCd
					0.625	-0.0156/-0.021	La2O3	Li2O	Li6Zr2O7	Li3Cd
					7.292	-0.0230/-0.027	La2O3	Li2O	Zr3O	Li3Cd
					7.625	-0.0232/-0.027	La2O3	Li2O	Zr4O	Li3Cd
					8.625	-0.0222	La2O3	Li2O	Zr	Li3Cd
Li56La23Zr16TlO96	La	Tl	3	-3.124	0.250	-0.0068/-0.022	La2O3	Li2O	Li6Zr2O7	Tl2O
					0.375	-0.0163/-0.031	La2O3	Li2O	Li6Zr2O7	Tl
					0.500	-0.0186/-0.033	La2O3	Li2O	Li6Zr2O7	LiTl
					0.625	-0.0198/-0.035	La2O3	Li2O	Li6Zr2O7	Li2Tl
					0.687	-0.0203/-0.035	La2O3	Li2O	Li6Zr2O7	Li5Tl2
					0.750	-0.0207/-0.035	La2O3	Li2O	Li6Zr2O7	Li3Tl
					7.417	-0.0270/-0.038	La2O3	Li2O	Zr3O	Li3Tl
					7.750	-0.0271/-0.038	La2O3	Li2O	Zr4O	Li3Tl
					8.750	-0.0261	La2O3	Li2O	Zr	Li3Tl
Li56La23Zr16InO96	La	In	3	-3.134	0.375	-0.0065/-0.021	La2O3	Li2O	Li6Zr2O7	In
					0.417	-0.0073/-0.022	La2O3	Li2O	Li6Zr2O7	LiIn3
					0.500	-0.0091/-0.024	La2O3	Li2O	Li6Zr2O7	LiIn
					0.562	-0.0101/-0.025	La2O3	Li2O	Li6Zr2O7	Li3In2
					0.625	-0.0108/-0.025	La2O3	Li2O	Li6Zr2O7	Li2In
					0.917	-0.0118/-0.026	La2O3	Li2O	Li6Zr2O7	Li13In3
					1.875	-0.0134/-0.027	La2O3	Li2O	Li6Zr2O7	Zr3In
					7.292	-0.0198/-0.031	La2O3	Li2O	Zr3O	Zr3In
					7.583	-0.0200/-0.031	La2O3	Li2O	Zr3O	Li13In3
					7.917	-0.0202/-0.031	La2O3	Li2O	Zr4O	Li13In3
					8.917	-0.0194	La2O3	Li2O	Zr	Li13In3
Li56La23Zr16SbO96	La	Sb	3	-3.136	0.375	-0.0045/-0.021	La2O3	Li2O	Li6Zr2O7	Sb
					0.625	-0.0135/-0.030	La2O3	Li2O	Li6Zr2O7	La2SbO2
					0.750	-0.0172/-0.033	La2O3	Li2O	Li6Zr2O7	Li3Sb
					7.417	-0.0243/-0.037	La2O3	Li2O	Zr3O	Li3Sb
					7.750	-0.0244/-0.037	La2O3	Li2O	Zr4O	Li3Sb
					8.750	-0.0235	La2O3	Li2O	Zr	Li3Sb
Li56La23Zr16BiO96	La	Bi	3	-3.135	0.375	-0.0055/-0.025	La2O3	Li2O	Li6Zr2O7	Bi
					0.625	-0.0140/-0.033	La2O3	Li2O	Li6Zr2O7	La2BiO2
					0.750	-0.0161/-0.035	La2O3	Li2O	Li6Zr2O7	Li3Bi
					7.417	-0.0234/-0.038	La2O3	Li2O	Zr3O	Li3Bi
					7.750	-0.0235/-0.038	La2O3	Li2O	Zr4O	Li3Bi
					8.750	-0.0226	La2O3	Li2O	Zr	Li3Bi

Li56La23Zr16AcO96	La	Ac	3	-3.165	0.375	0.0240	La2O3	Li2O	Li6Zr2O7	Ac
					6.667	0.0079/-0.011	La2O3	Li2O	Zr3O	Ac2O3
					7.000	0.0074/-0.011	La2O3	Li2O	Zr4O	Ac2O3
					8.000	0.0074	La2O3	Li2O	Zr	Ac2O3
Li56La23Zr16DyO96	La	Dy	3	-3.165	0.375	0.0240	La2O3	Li2O	Li6Zr2O7	Dy
					6.667	0.0049/-0.011	La2O3	Li2O	Zr3O	LiDyO2
					7.000	0.0044/-0.011	La2O3	Li2O	Zr4O	LiDyO2
					8.000	0.0045	La2O3	Li2O	Zr	LiDyO2
Li56La23Zr16ErO96	La	Er	3	-3.165	0.375	0.0240	La2O3	Li2O	Li6Zr2O7	Er
					6.667	0.0044/-0.011	La2O3	Li2O	Zr3O	LiErO2
					7.000	0.0040/-0.011	La2O3	Li2O	Zr4O	LiErO2
					8.000	0.0041	La2O3	Li2O	Zr	LiErO2
Li56La23Zr16GdO96	La	Gd	3	-3.165	0.375	0.0240	La2O3	Li2O	Li6Zr2O7	Gd
					6.667	0.0063/-0.011	La2O3	Li2O	Zr3O	LiGdO2
					7.000	0.0058/-0.011	La2O3	Li2O	Zr4O	LiGdO2
					8.000	0.0058	La2O3	Li2O	Zr	LiGdO2
Li56La23Zr16HoO96	La	Ho	3	-3.165	0.375	0.0240	La2O3	Li2O	Li6Zr2O7	Ho
					6.667	0.0047/-0.011	La2O3	Li2O	Zr3O	LiHoO2
					7.000	0.0043/-0.011	La2O3	Li2O	Zr4O	LiHoO2
					8.000	0.0044	La2O3	Li2O	Zr	LiHoO2
Li56La23Zr16LuO96	La	Lu	3	-3.165	0.375	0.0240	La2O3	Li2O	Li6Zr2O7	Lu
					6.667	0.0033/-0.011	La2O3	Li2O	Zr3O	LiLuO2
					7.000	0.0029/-0.011	La2O3	Li2O	Zr4O	LiLuO2
					8.000	0.0031	La2O3	Li2O	Zr	LiLuO2
Li56La23Zr16NdO96	La	Nd	3	-3.165	0.375	0.0240	La2O3	Li2O	Li6Zr2O7	Nd
					6.667	0.0074/-0.011	La2O3	Li2O	Zr3O	Nd2O3
					7.000	0.0069/-0.011	La2O3	Li2O	Zr4O	Nd2O3
					8.000	0.0069	La2O3	Li2O	Zr	Nd2O3
Li56La23Zr16PmO96	La	Pm	3	-3.165	0.375	0.0240	La2O3	Li2O	Li6Zr2O7	Pm
					6.667	0.0068/-0.011	La2O3	Li2O	Zr3O	Pm2O3
					7.000	0.0064/-0.011	La2O3	Li2O	Zr4O	Pm2O3
					8.000	0.0064	La2O3	Li2O	Zr	Pm2O3
Li56La23Zr16PrO96	La	Pr	3	-3.164	0.375	0.0230	La2O3	Li2O	Li6Zr2O7	Pr
					6.667	0.0071/-0.011	La2O3	Li2O	Zr3O	Pr2O3
					7.000	0.0067/-0.011	La2O3	Li2O	Zr4O	Pr2O3
					8.000	0.0067	La2O3	Li2O	Zr	Pr2O3
Li56La23Zr16SmO96	La	Sm	3	-3.165	0.375	0.0240	La2O3	Li2O	Li6Zr2O7	Sm
					6.667	0.0066/-0.011	La2O3	Li2O	Zr3O	Sm2O3
					7.000	0.0061/-0.011	La2O3	Li2O	Zr4O	Sm2O3
					8.000	0.0062	La2O3	Li2O	Zr	Sm2O3
Li56La23Zr16TbO96	La	Tb	3	-3.165	0.375	0.0240	La2O3	Li2O	Li6Zr2O7	Tb

					6.667	0.0052/-0.011	La2O3	Li2O	Zr3O	LiTbO2
					7.000	0.0048/-0.011	La2O3	Li2O	Zr4O	LiTbO2
					8.000	0.0048	La2O3	Li2O	Zr	LiTbO2
Li56La23Zr16TmO96	La	Tm	3	-3.165	0.375	0.0240	La2O3	Li2O	Li6Zr2O7	Tm
					6.667	0.0039/-0.011	La2O3	Li2O	Zr3O	LiTmO2
					7.000	0.0035/-0.011	La2O3	Li2O	Zr4O	LiTmO2
					8.000	0.0036	La2O3	Li2O	Zr	LiTmO2
Li56La23Zr16CeO96	La	Ce	3	-3.163	0.125	0.0209/-0.001	La2O3	Li2O	Li6Zr2O7	CeO
					6.792	0.0054/-0.011	La2O3	Li2O	Zr3O	CeO
					7.125	0.0050/-0.011	La2O3	Li2O	Zr4O	CeO
					8.125	0.0050	La2O3	Li2O	Zr	CeO
Li56La23Zr16YbO96	La	Yb	3	-3.150	0.125	0.0037/-0.015	La2O3	Li2O	Li6Zr2O7	YbO
					6.792	-0.0080/-0.022	La2O3	Li2O	Zr3O	YbO
					7.125	-0.0083/-0.023	La2O3	Li2O	Zr4O	YbO
					8.125	-0.0078	La2O3	Li2O	Zr	YbO
Li56La23Zr16YO96	La	Y	3	-3.165	0.375	0.0240	La2O3	Li2O	Li6Zr2O7	Y
					6.667	0.0055/-0.011	La2O3	Li2O	Zr3O	LiYO2
					7.000	0.0050/-0.011	La2O3	Li2O	Zr4O	LiYO2
					8.000	0.0051	La2O3	Li2O	Zr	LiYO2
Li56La23Zr16NO96	La	N	3	-3.109	0.375	-0.0311/-0.035	La2O3	Li2O	Li6Zr2O7	N2
					0.417	-0.0339/-0.037	La2O3	Li2O	Li6Zr2O7	LiN3
					0.750	-0.0471/-0.051	La2O3	Li2O	Li6Zr2O7	Li2ZrN2
					0.875	-0.0501/-0.054	La2O3	Li2O	Li6Zr2O7	ZrN
					1.375	-0.0514/-0.055	La2O3	Li2O	Li6Zr2O7	Zr2N
					7.208	-0.0513/-0.054	La2O3	Li2O	Zr3O	Zr2N
					7.500	-0.0511/-0.054	La2O3	Li2O	Zr4O	Zr2N
					8.375	-0.0495	La2O3	Li2O	Zr	Zr2N
Li56La23Zr16ScO96	La	Sc	3	-3.160	0.375	0.0191	La2O3	Li2O	Li6Zr2O7	Sc
					6.667	0.0001/-0.011	La2O3	Li2O	Zr3O	LiScO2
					7.000	-0.0003/-0.011	La2O3	Li2O	Zr4O	LiScO2
					8.000	0.0	La2O3	Li2O	Zr	LiScO2
Li58La24Zr15CdO96	Zr	Cd	2	-3.101	0.250	-0.0100/-0.018	La2O3	Li2O	Li6Zr2O7	Cd
					0.292	-0.0112/-0.019	La2O3	Li2O	Li6Zr2O7	LiCd3
					0.375	-0.0125/-0.020	La2O3	Li2O	Li6Zr2O7	LiCd
					0.625	-0.0134/-0.021	La2O3	Li2O	Li6Zr2O7	Li3Cd
					6.875	-0.0209/-0.027	La2O3	Li2O	Zr3O	Li3Cd
					7.187	-0.0210/-0.027	La2O3	Li2O	Zr4O	Li3Cd
					8.125	-0.0202	La2O3	Li2O	Zr	Li3Cd
Li58La24Zr15HgO96	Zr	Hg	2	-3.091	0.250	-0.0199/-0.023	La2O3	Li2O	Li6Zr2O7	Hg
					0.375	-0.0235/-0.027	La2O3	Li2O	Li6Zr2O7	LiHg
					0.625	-0.0252/-0.028	La2O3	Li2O	Li6Zr2O7	Li3Hg

					6.875	-0.0303/-0.032	La2O3	Li2O	Zr3O	Li3Hg
					7.187	-0.0303/-0.032	La2O3	Li2O	Zr4O	Li3Hg
					8.125	-0.0293	La2O3	Li2O	Zr	Li3Hg
Li58La24Zr15MgO96	Zr	Mg	2	-3.117	0.375	0.0052/-0.001	La2O3	Li2O	Li6Zr2O7	LiMg
					0.625	0.0051	La2O3	Li2O	Li6Zr2O7	Li3Mg
					0.875	0.0050	La2O3	Li2O	Li6Zr2O7	Li5Mg
					6.625	-0.0061/-0.011	La2O3	Li2O	Zr3O	LiMg
					6.937	-0.0064/-0.011	La2O3	Li2O	Zr4O	LiMg
					7.187	-0.0064/-0.011	La2O3	Li2O	Zr4O	Li3Mg
					7.437	-0.0063/-0.011	La2O3	Li2O	Zr4O	Li5Mg
					8.375	-0.0059	La2O3	Li2O	Zr	Li5Mg
Li58La24Zr15CuO96	Zr	Cu	2	-3.095	0.125	-0.0063/-0.011	La2O3	Li2O	Li6Zr2O7	LiCuO
					0.250	-0.0159/-0.020	La2O3	Li2O	Li6Zr2O7	Cu
					0.387	-0.0171/-0.022	La2O3	Li2O	Li6Zr2O7	Zr14Cu51
					1.250	-0.0190/-0.023	La2O3	Li2O	Li6Zr2O7	Zr2Cu
					6.667	-0.0245/-0.028	La2O3	Li2O	Zr3O	Zr2Cu
					6.937	-0.0246/-0.028	La2O3	Li2O	Zr4O	Zr2Cu
					7.750	-0.0238	La2O3	Li2O	Zr	Zr2Cu
Li58La24Zr15NiO96	Zr	Ni	2	-3.094	0.250	-0.0169/-0.022	La2O3	Li2O	Li6Zr2O7	Ni
					0.393	-0.0199/-0.025	La2O3	Li2O	Li6Zr2O7	Zr2Ni7
					0.417	-0.0201/-0.025	La2O3	Li2O	Li6Zr2O7	ZrNi3
					0.750	-0.0220/-0.027	La2O3	Li2O	Li6Zr2O7	ZrNi
					1.250	-0.0227/-0.028	La2O3	Li2O	Li6Zr2O7	Zr2Ni
					6.667	-0.0275/-0.031	La2O3	Li2O	Zr3O	Zr2Ni
					6.937	-0.0276/-0.031	La2O3	Li2O	Zr4O	Zr2Ni
					7.750	-0.0268	La2O3	Li2O	Zr	Zr2Ni
Li58La24Zr15EuO96	Zr	Eu	2	-3.094	0.250	-0.0169	La2O3	Li2O	Li6Zr2O7	Eu
					6.250	-0.0242/-0.010	La2O3	Li2O	Zr3O	EuO
					6.562	-0.0243/-0.010	La2O3	Li2O	Zr4O	EuO
					7.500	-0.0234	La2O3	Li2O	Zr	EuO
Li58La24Zr15CaO96	Zr	Ca	2	-3.122	0.250	0.0108	La2O3	Li2O	Li6Zr2O7	Ca
					6.250	-0.0034/-0.010	La2O3	Li2O	Zr3O	CaO
					6.562	-0.0037/-0.010	La2O3	Li2O	Zr4O	CaO
					7.500	-0.0034	La2O3	Li2O	Zr	CaO
Li58La24Zr15BeO96	Zr	Be	2	-3.115	0.288	0.0027	La2O3	Li2O	Li6Zr2O7	ZrBe13
					0.309	0.0024	La2O3	Li2O	Li6Zr2O7	Zr2Be17
					0.350	0.0022/-0.002	La2O3	Li2O	Li6Zr2O7	ZrBe5
					6.517	-0.0084/-0.011	La2O3	Li2O	Zr3O	ZrBe5
					6.825	-0.0087/-0.011	La2O3	Li2O	Zr4O	ZrBe5
					7.750	-0.0082	La2O3	Li2O	Zr	ZrBe5
Li58La24Zr15ZnO96	Zr	Zn	2	-3.104	0.250	-0.0070/-0.012	La2O3	Li2O	Li6Zr2O7	Zn

					0.279	-0.0079/-0.013	La2O3	Li2O	Li6Zr2O7	LaZn13
					0.284	-0.0081/-0.013	La2O3	Li2O	Li6Zr2O7	LaZn11
					0.294	-0.0082/-0.013	La2O3	Li2O	Li6Zr2O7	La2Zn17
					0.375	-0.0091/-0.014	La2O3	Li2O	Li6Zr2O7	LiZn
					0.417	-0.0092	La2O3	Li2O	Li6Zr2O7	ZrZn3
					0.500	-0.0096	La2O3	Li2O	Li6Zr2O7	ZrZn2
					0.750	-0.0105/-0.015	La2O3	Li2O	Li6Zr2O7	ZrZn
					6.583	-0.0181/-0.022	La2O3	Li2O	Zr3O	ZrZn
					6.875	-0.0183/-0.022	La2O3	Li2O	Zr4O	ZrZn
					7.750	-0.0176	La2O3	Li2O	Zr	ZrZn
Li58La24Zr15MnO96	Zr	Mn	2	-3.093	0.250	-0.0179/-0.011	La2O3	Li2O	Li6Zr2O7	Mn
					0.500	-0.0196/-0.013	La2O3	Li2O	Li6Zr2O7	ZrMn2
					6.542	-0.0256/-0.020	La2O3	Li2O	Zr3O	ZrMn2
					6.844	-0.0258/-0.020	La2O3	Li2O	Zr4O	ZrMn2
					7.750	-0.0248	La2O3	Li2O	Zr	ZrMn2
Li58La24Zr15SrO96	Zr	Sr	2	-3.118	0.250	0.0068	La2O3	Li2O	Li6Zr2O7	Sr
					6.250	-0.0047/-0.010	La2O3	Li2O	Zr3O	SrO
					6.562	-0.0051/-0.010	La2O3	Li2O	Zr4O	SrO
					6.812	-0.0052/-0.010	La2O3	Li2O	Zr4O	Sr
					6.896	-0.0051/-0.010	La2O3	Li2O	Zr4O	Sr3Li2
					7.833	-0.0048	La2O3	Li2O	Zr	Sr3Li2
Li58La24Zr15FeO96	Zr	Fe	2	-3.093	0.250	-0.0179/-0.013	La2O3	Li2O	Li6Zr2O7	Fe
					0.500	-0.0203/-0.016	La2O3	Li2O	Li6Zr2O7	ZrFe2
					1.750	-0.0218/-0.017	La2O3	Li2O	Li6Zr2O7	Zr3Fe
					6.750	-0.0264/-0.022	La2O3	Li2O	Zr3O	Zr3Fe
					7.000	-0.0265/-0.022	La2O3	Li2O	Zr4O	Zr3Fe
					7.750	-0.0257	La2O3	Li2O	Zr	Zr3Fe
Li58La24Zr15CoO96	Zr	Co	2	-3.095	0.250	-0.0159/-0.017	La2O3	Li2O	Li6Zr2O7	Co
					0.380	-0.0175/-0.018	La2O3	Li2O	Li6Zr2O7	Zr6Co23
					0.500	-0.0185/-0.019	La2O3	Li2O	Li6Zr2O7	ZrCo2
					0.750	-0.0193/-0.020	La2O3	Li2O	Li6Zr2O7	ZrCo
					1.250	-0.0208/-0.022	La2O3	Li2O	Li6Zr2O7	Zr2Co
					1.750	-0.0215/-0.022	La2O3	Li2O	Li6Zr2O7	Zr3Co
					6.750	-0.0262/-0.027	La2O3	Li2O	Zr3O	Zr3Co
					7.000	-0.0263/-0.027	La2O3	Li2O	Zr4O	Zr3Co
					7.750	-0.0255	La2O3	Li2O	Zr	Zr3Co
Li57La24Zr15FeO96	Zr	Fe	3	-3.125	0.375	-0.0022/-0.020	La2O3	Li2O	Li6Zr2O7	Fe
					0.625	-0.0047/-0.022	La2O3	Li2O	Li6Zr2O7	ZrFe2
					1.875	-0.0070/-0.023	La2O3	Li2O	Li6Zr2O7	Zr3Fe
					6.875	-0.0140/-0.027	La2O3	Li2O	Zr3O	Zr3Fe
					7.125	-0.0142/-0.028	La2O3	Li2O	Zr4O	Zr3Fe

					7.875	-0.0137	La2O3	Li2O	Zr	Zr3Fe
Li57La24Zr15InO96	Zr	In	3	-3.127	0.417	-0.0011/-0.022	La2O3	Li2O	Li6Zr2O7	LiIn3
					0.500	-0.0028/-0.024	La2O3	Li2O	Li6Zr2O7	LiIn
					0.562	-0.0039/-0.025	La2O3	Li2O	Li6Zr2O7	Li3In2
					0.625	-0.0046/-0.025	La2O3	Li2O	Li6Zr2O7	Li2In
					0.917	-0.0057/-0.026	La2O3	Li2O	Li6Zr2O7	Li13In3
					1.875	-0.0074/-0.027	La2O3	Li2O	Li6Zr2O7	Zr3In
					6.875	-0.0144/-0.030	La2O3	Li2O	Zr3O	Zr3In
					7.167	-0.0146/-0.031	La2O3	Li2O	Zr3O	Li13In3
					7.479	-0.0149/-0.031	La2O3	Li2O	Zr4O	Li13In3
					8.417	-0.0142	La2O3	Li2O	Zr	Li13In3
Li57La24Zr15RhO96	Zr	Rh	3	-3.115	0.375	-0.0120/-0.031	La2O3	Li2O	Li6Zr2O7	Rh
					0.542	-0.0168/-0.035	La2O3	Li2O	Li6Zr2O7	ZrRh3
					0.675	-0.0189/-0.037	La2O3	Li2O	Li6Zr2O7	Zr3Rh5
					0.875	-0.0207/-0.039	La2O3	Li2O	Li6Zr2O7	ZrRh
					1.375	-0.0214/-0.039	La2O3	Li2O	Li6Zr2O7	Zr2Rh
					6.792	-0.0265/-0.041	La2O3	Li2O	Zr3O	Zr2Rh
					7.062	-0.0266/-0.041	La2O3	Li2O	Zr4O	Zr2Rh
					7.875	-0.0257	La2O3	Li2O	Zr	Zr2Rh
Li57La24Zr15ScO96	Zr	Sc	3	-3.154	0.375	0.0264	La2O3	Li2O	Li6Zr2O7	Sc
					6.250	0.0067/-0.010	La2O3	Li2O	Zr3O	LiScO2
					6.562	0.0063/-0.010	La2O3	Li2O	Zr4O	LiScO2
					7.500	0.0063	La2O3	Li2O	Zr	LiScO2
Li57La24Zr15TlO96	Zr	Tl	3	-3.115	0.250	-0.0025/-0.022	La2O3	Li2O	Li6Zr2O7	Tl2O
					0.375	-0.0120/-0.031	La2O3	Li2O	Li6Zr2O7	Tl
					0.500	-0.0143/-0.033	La2O3	Li2O	Li6Zr2O7	LiTl
					0.625	-0.0155/-0.034	La2O3	Li2O	Li6Zr2O7	Li2Tl
					0.687	-0.0160/-0.035	La2O3	Li2O	Li6Zr2O7	Li5Tl2
					0.750	-0.0164/-0.035	La2O3	Li2O	Li6Zr2O7	Li3Tl
					7.000	-0.0233/-0.038	La2O3	Li2O	Zr3O	Li3Tl
					7.312	-0.0234/-0.038	La2O3	Li2O	Zr4O	Li3Tl
					8.250	-0.0225	La2O3	Li2O	Zr	Li3Tl
Li57La24Zr15AuO96	Zr	Au	3	-3.106	0.375	-0.0209/-0.034	La2O3	Li2O	Li6Zr2O7	Au
					0.417	-0.0233/-0.037	La2O3	Li2O	Li6Zr2O7	LiAu3
					0.500	-0.0264/-0.040	La2O3	Li2O	Li6Zr2O7	LiAu
					0.750	-0.0287/-0.042	La2O3	Li2O	Li6Zr2O7	Li3Au
					0.844	-0.0288/-0.042	La2O3	Li2O	Li6Zr2O7	Li15Au4
					7.094	-0.0332/-0.043	La2O3	Li2O	Zr3O	Li15Au4
					7.406	-0.0332/-0.043	La2O3	Li2O	Zr4O	Li15Au4
					8.344	-0.0321	La2O3	Li2O	Zr	Li15Au4
Li57La24Zr15CrO96	Zr	Cr	3	-3.125	0.375	-0.0022/-0.014	La2O3	Li2O	Li6Zr2O7	Cr

					0.625	-0.0029/-0.015	La2O3	Li2O	Li6Zr2O7	ZrCr2
					6.667	-0.0123/-0.022	La2O3	Li2O	Zr3O	ZrCr2
					6.969	-0.0125/-0.022	La2O3	Li2O	Zr4O	ZrCr2
					7.875	-0.0120	La2O3	Li2O	Zr	ZrCr2
Li57La24Zr15PO96	Zr	P	3	-3.127	0.750	-0.0145/-0.021	La2O3	Li2O	Li6Zr2O7	Li3LaP2
					1.153	-0.0171/-0.023	La2O3	Li2O	Li6Zr2O7	Zr14P9
					1.250	-0.0175/-0.024	La2O3	Li2O	Li6Zr2O7	Zr7P4
					1.875	-0.0196/-0.026	La2O3	Li2O	Li6Zr2O7	Zr3P
					6.875	-0.0246/-0.029	La2O3	Li2O	Zr3O	Zr3P
					7.125	-0.0247/-0.030	La2O3	Li2O	Zr4O	Zr3P
					7.875	-0.0240	La2O3	Li2O	Zr	Zr3P
Li57La24Zr15AlO96	Zr	Al	3	-3.145	0.542	0.0138	La2O3	Li2O	Li6Zr2O7	ZrAl3
					0.625	0.0128/-0.003	La2O3	Li2O	Li6Zr2O7	ZrAl2
					0.708	0.0123/-0.004	La2O3	Li2O	Li6Zr2O7	Zr2Al3
					1.042	0.0105/-0.005	La2O3	Li2O	Li6Zr2O7	Zr4Al3
					1.875	0.0083/-0.007	La2O3	Li2O	Li6Zr2O7	Zr3Al
					6.875	-0.0012/-0.014	La2O3	Li2O	Zr3O	Zr3Al
					7.125	-0.0015/-0.014	La2O3	Li2O	Zr4O	Zr3Al
					7.875	-0.0013	La2O3	Li2O	Zr	Zr3Al
Li57La24Zr15GaO96	Zr	Ga	3	-3.129	0.375	0.0017/-0.013	La2O3	Li2O	Li6Zr2O7	Ga
					0.411	0.0006/-0.014	La2O3	Li2O	Li6Zr2O7	Li2Ga7
					0.437	-0.0001/-0.015	La2O3	Li2O	Li6Zr2O7	LaGa6
					0.500	-0.0015/-0.016	La2O3	Li2O	Li6Zr2O7	LiGa
					0.562	-0.0025/-0.017	La2O3	Li2O	Li6Zr2O7	LaGa2
					0.708	-0.0040/-0.019	La2O3	Li2O	Li6Zr2O7	Zr2Ga3
					0.875	-0.0054/-0.020	La2O3	Li2O	Li6Zr2O7	ZrGa
					1.125	-0.0063/-0.021	La2O3	Li2O	Li6Zr2O7	Zr3Ga2
					1.375	-0.0068/-0.021	La2O3	Li2O	Li6Zr2O7	Zr2Ga
					6.792	-0.0145/-0.026	La2O3	Li2O	Zr3O	Zr2Ga
					7.062	-0.0147/-0.026	La2O3	Li2O	Zr4O	Zr2Ga
					7.875	-0.0141	La2O3	Li2O	Zr	Zr2Ga
Li57La24Zr15TmO96	Zr	Tm	3	-3.155	0.375	0.0273	La2O3	Li2O	Li6Zr2O7	Tm
					6.250	0.0074/-0.010	La2O3	Li2O	Zr3O	LiTmO2
					6.562	0.0070/-0.010	La2O3	Li2O	Zr4O	LiTmO2
					7.500	0.0070	La2O3	Li2O	Zr	LiTmO2
Li57La24Zr15DyO96	Zr	Dy	3	-3.153	0.375	0.0254	La2O3	Li2O	Li6Zr2O7	Dy
					6.250	0.0068/-0.010	La2O3	Li2O	Zr3O	LiDyO2
					6.562	0.0064/-0.010	La2O3	Li2O	Zr4O	LiDyO2
					7.500	0.0064	La2O3	Li2O	Zr	LiDyO2
Li57La24Zr15BiO96	Zr	Bi	3	-3.120	0.375	-0.0071/-0.025	La2O3	Li2O	Li6Zr2O7	Bi
					0.625	-0.0156/-0.033	La2O3	Li2O	Li6Zr2O7	La2BiO2

					0.750	-0.0176/-0.035	La2O3	Li2O	Li6Zr2O7	Li3Bi
					7.000	-0.0242/-0.038	La2O3	Li2O	Zr3O	Li3Bi
					7.312	-0.0243/-0.038	La2O3	Li2O	Zr4O	Li3Bi
					8.250	-0.0234	La2O3	Li2O	Zr	Li3Bi
Li57La24Zr15YO96	Zr	Y	3	-3.154	0.375	0.0264	La2O3	Li2O	Li6Zr2O7	Y
					6.250	0.0082/-0.010	La2O3	Li2O	Zr3O	LiYO2
					6.562	0.0077/-0.010	La2O3	Li2O	Zr4O	LiYO2
					7.500	0.0077	La2O3	Li2O	Zr	LiYO2
Li57La24Zr15TbO96	Zr	Tb	3	-3.153	0.375	0.0254	La2O3	Li2O	Li6Zr2O7	Tb
					6.250	0.0071/-0.010	La2O3	Li2O	Zr3O	LiTbO2
					6.562	0.0067/-0.010	La2O3	Li2O	Zr4O	LiTbO2
					7.500	0.0067	La2O3	Li2O	Zr	LiTbO2
Li57La24Zr15NdO96	Zr	Nd	3	-3.149	0.375	0.0214	La2O3	Li2O	Li6Zr2O7	Nd
					6.250	0.0062/-0.010	La2O3	Li2O	Zr3O	Nd2O3
					6.562	0.0057/-0.010	La2O3	Li2O	Zr4O	Nd2O3
					7.500	0.0058	La2O3	Li2O	Zr	Nd2O3
Li57La24Zr15SmO96	Zr	Sm	3	-3.150	0.375	0.0224	La2O3	Li2O	Li6Zr2O7	Sm
					6.250	0.0061/-0.010	La2O3	Li2O	Zr3O	Sm2O3
					6.562	0.0057/-0.010	La2O3	Li2O	Zr4O	Sm2O3
					7.500	0.0057	La2O3	Li2O	Zr	Sm2O3
Li57La24Zr15PmO96	Zr	Pm	3	-3.150	0.375	0.0224	La2O3	Li2O	Li6Zr2O7	Pm
					6.250	0.0064/-0.010	La2O3	Li2O	Zr3O	Pm2O3
					6.562	0.0060/-0.010	La2O3	Li2O	Zr4O	Pm2O3
					7.500	0.0060	La2O3	Li2O	Zr	Pm2O3
Li57La24Zr15CeO96	Zr	Ce	3	-3.147	0.125	0.0183/-0.001	La2O3	Li2O	Li6Zr2O7	CeO
					6.375	0.0042/-0.011	La2O3	Li2O	Zr3O	CeO
					6.687	0.0038/-0.011	La2O3	Li2O	Zr4O	CeO
					7.625	0.0039	La2O3	Li2O	Zr	CeO
Li57La24Zr15IrO96	Zr	Ir	3	-3.112	0.375	-0.0150/-0.031	La2O3	Li2O	Li6Zr2O7	Ir
					0.542	-0.0199/-0.036	La2O3	Li2O	Li6Zr2O7	ZrIr3
					0.875	-0.0240/-0.040	La2O3	Li2O	Li6Zr2O7	ZrIr
					1.208	-0.0255/-0.041	La2O3	Li2O	Li6Zr2O7	Zr5Ir3
					1.875	-0.0266/-0.042	La2O3	Li2O	Li6Zr2O7	Zr3Ir
					6.875	-0.0304/-0.043	La2O3	Li2O	Zr3O	Zr3Ir
					7.125	-0.0305/-0.043	La2O3	Li2O	Zr4O	Zr3Ir
					7.875	-0.0296	La2O3	Li2O	Zr	Zr3Ir
Li57La24Zr15HoO96	Zr	Ho	3	-3.154	0.375	0.0264	La2O3	Li2O	Li6Zr2O7	Ho
					6.250	0.0074/-0.010	La2O3	Li2O	Zr3O	LiHoO2
					6.562	0.0070/-0.010	La2O3	Li2O	Zr4O	LiHoO2
					7.500	0.0070	La2O3	Li2O	Zr	LiHoO2
Li57La24Zr15ErO96	Zr	Er	3	-3.154	0.375	0.0264	La2O3	Li2O	Li6Zr2O7	Er

					6.250	0.0071/-0.010	La2O3	Li2O	Zr3O	LiErO2
					6.562	0.0067/-0.010	La2O3	Li2O	Zr4O	LiErO2
					7.500	0.0067	La2O3	Li2O	Zr	LiErO2
Li57La24Zr15GdO96	Zr	Gd	3	-3.152	0.375	0.0244	La2O3	Li2O	Li6Zr2O7	Gd
					6.250	0.0074/-0.010	La2O3	Li2O	Zr3O	LiGdO2
					6.562	0.0069/-0.010	La2O3	Li2O	Zr4O	LiGdO2
					7.500	0.0069	La2O3	Li2O	Zr	LiGdO2
Li57La24Zr15RuO96	Zr	Ru	3	-3.113	0.375	-0.0140/-0.028	La2O3	Li2O	Li6Zr2O7	Ru
					0.875	-0.0211/-0.035	La2O3	Li2O	Li6Zr2O7	ZrRu
					6.708	-0.0267/-0.038	La2O3	Li2O	Zr3O	ZrRu
					7.000	-0.0268/-0.038	La2O3	Li2O	Zr4O	ZrRu
					7.875	-0.0259	La2O3	Li2O	Zr	ZrRu
Li56La24Zr15CO96	Zr	C	4	-3.089	0.500	-0.0534/-0.026	La2O3	Li2O	Li6Zr2O7	C
					1.000	-0.0613/-0.034	La2O3	Li2O	Li6Zr2O7	ZrC
					1.056	-0.0616/-0.035	La2O3	Li2O	Li6Zr2O7	Zr10C9
					6.843	-0.0595/-0.037	La2O3	Li2O	Zr3O	Zr10C9
					7.132	-0.0593/-0.037	La2O3	Li2O	Zr4O	Zr10C9
					8.000	-0.0575	La2O3	Li2O	Zr	Zr10C9
Li56La24Zr15GeO96	Zr	Ge	4	-3.099	0.500	-0.0436/-0.021	La2O3	Li2O	Li6Zr2O7	Ge
					0.625	-0.0462	La2O3	Li2O	Li6Zr2O7	LiGe
					0.705	-0.0479	La2O3	Li2O	Li6Zr2O7	La6Ge11
					0.750	-0.0492/-0.027	La2O3	Li2O	Li6Zr2O7	LiLaGe2
					1.000	-0.0516	La2O3	Li2O	Li6Zr2O7	ZrGe
					1.125	-0.0530/-0.031	La2O3	Li2O	Li6Zr2O7	Zr5Ge4
					1.333	-0.0541/-0.032	La2O3	Li2O	Li6Zr2O7	Zr5Ge3
					2.000	-0.0541/-0.032	La2O3	Li2O	Li6Zr2O7	Zr3Ge
					7.000	-0.0535/-0.035	La2O3	Li2O	Zr3O	Zr3Ge
					7.250	-0.0534/-0.035	La2O3	Li2O	Zr4O	Zr3Ge
					8.000	-0.0519	La2O3	Li2O	Zr	Zr3Ge
Li56La24Zr15HfO96	Zr	Hf	4	-3.131	0.500	-0.0123	La2O3	Li2O	Li6Zr2O7	Hf
					1.000	-0.0128	La2O3	Li2O	Li6Zr2O7	HfZr
					6.250	-0.0228/-0.010	La2O3	Li2O	Zr3O	Li6Hf2O7
					6.562	-0.0230/-0.010	La2O3	Li2O	Zr4O	Li6Hf2O7
					7.500	-0.0221	La2O3	Li2O	Zr	Li6Hf2O7
Li56La24Zr15MoO96	Zr	Mo	4	-3.097	0.500	-0.0456/-0.027	La2O3	Li2O	Li6Zr2O7	Mo
					0.750	-0.0465/-0.028	La2O3	Li2O	Li6Zr2O7	ZrMo2
					6.792	-0.0473/-0.032	La2O3	Li2O	Zr3O	ZrMo2
					7.094	-0.0472/-0.032	La2O3	Li2O	Zr4O	ZrMo2
					8.000	-0.0456	La2O3	Li2O	Zr	ZrMo2
Li56La24Zr15PbO96	Zr	Pb	4	-3.088	0.250	-0.0382/-0.022	La2O3	Li2O	Li6Zr2O7	PbO
					0.500	-0.0544/-0.038	La2O3	Li2O	Li6Zr2O7	Pb

					0.625	-0.0569/-0.041	La2O3	Li2O	Li6Zr2O7	LiPb
					0.833	-0.0596/-0.044	La2O3	Li2O	Li6Zr2O7	Li8Pb3
					0.875	-0.0600/-0.044	La2O3	Li2O	Li6Zr2O7	Li3Pb
					0.937	-0.0605/-0.045	La2O3	Li2O	Li6Zr2O7	Li7Pb2
					1.031	-0.0608/-0.045	La2O3	Li2O	Li6Zr2O7	Li17Pb4
					7.281	-0.0587/-0.046	La2O3	Li2O	Zr3O	Li17Pb4
					7.594	-0.0585/-0.046	La2O3	Li2O	Zr4O	Li17Pb4
					8.531	-0.0566	La2O3	Li2O	Zr	Li17Pb4
Li56La24Zr15PdO96	Zr	Pd	4	-3.081	0.250	-0.0400/-0.024	La2O3	Li2O	Li6Zr2O7	Li2PdO2
					0.500	-0.0612/-0.045	La2O3	Li2O	Li6Zr2O7	Pd
					0.518	-0.0622/-0.046	La2O3	Li2O	Li6Zr2O7	LiPd7
					0.575	-0.0642/-0.048	La2O3	Li2O	Li6Zr2O7	LaPd5
					0.625	-0.0658/-0.050	La2O3	Li2O	Li6Zr2O7	LaPd3
					0.667	-0.0666/-0.050	La2O3	Li2O	Li6Zr2O7	ZrPd3
					1.000	-0.0673/-0.051	La2O3	Li2O	Li6Zr2O7	ZrPd
					1.500	-0.0677/-0.052	La2O3	Li2O	Li6Zr2O7	Zr2Pd
					6.917	-0.0647/-0.051	La2O3	Li2O	Zr3O	Zr2Pd
					7.187	-0.0644/-0.051	La2O3	Li2O	Zr4O	Zr2Pd
					8.000	-0.0626	La2O3	Li2O	Zr	Zr2Pd
Li56La24Zr15PtO96	Zr	Pt	4	-3.083	0.500	-0.0593/-0.043	La2O3	Li2O	Li6Zr2O7	Pt
					0.518	-0.0607/-0.044	La2O3	Li2O	Li6Zr2O7	LiPt7
					0.542	-0.0620/-0.046	La2O3	Li2O	Li6Zr2O7	LiPt3
					0.575	-0.0634/-0.047	La2O3	Li2O	Li6Zr2O7	LaPt5
					0.625	-0.0651/-0.049	La2O3	Li2O	Li6Zr2O7	LiPt
					0.667	-0.0661/-0.050	La2O3	Li2O	Li6Zr2O7	ZrPt3
					0.812	-0.0678/-0.052	La2O3	Li2O	Li6Zr2O7	LiZrPt2
					1.000	-0.0698/-0.054	La2O3	Li2O	Li6Zr2O7	ZrPt
					6.833	-0.0661/-0.053	La2O3	Li2O	Zr3O	ZrPt
					7.125	-0.0659/-0.053	La2O3	Li2O	Zr4O	ZrPt
					8.000	-0.0639	La2O3	Li2O	Zr	ZrPt
Li56La24Zr15SO96	Zr	S	4	-3.088	0.667	-0.0658	La2O3	Li2O	Li6Zr2O7	ZrS3
					0.750	-0.0780/-0.048	La2O3	Li2O	Li6Zr2O7	La2SO2
					7.000	-0.0724/-0.048	La2O3	Li2O	Zr3O	La2SO2
					7.312	-0.0721/-0.048	La2O3	Li2O	Zr4O	La2SO2
					8.250	-0.0698	La2O3	Li2O	Zr	La2SO2
Li56La24Zr15SiO96	Zr	Si	4	-3.112	0.750	-0.0359	La2O3	Li2O	Li6Zr2O7	ZrSi2
					1.000	-0.0404/-0.013	La2O3	Li2O	Li6Zr2O7	ZrSi
					1.125	-0.0413	La2O3	Li2O	Li6Zr2O7	Zr5Si4
					1.250	-0.0422/-0.015	La2O3	Li2O	Li6Zr2O7	Zr3Si2
					1.500	-0.0428/-0.016	La2O3	Li2O	Li6Zr2O7	Zr2Si
					6.917	-0.0441/-0.022	La2O3	Li2O	Zr3O	Zr2Si

					7.187	-0.0441/-0.022	La2O3	Li2O	Zr4O	Zr2Si
					8.000	-0.0428	La2O3	Li2O	Zr	Zr2Si
Li56La24Zr15SnO96	Zr	Sn	4	-3.100	0. 500	-0.0426/-0.025	La2O3	Li2O	Li6Zr2O7	Sn
					0.625	-0.0457/-0.029	La2O3	Li2O	Li6Zr2O7	LiSn
					0.825	-0.0494/-0.032	La2O3	Li2O	Li6Zr2O7	Li13Sn5
					0.937	-0.0503/-0.033	La2O3	Li2O	Li6Zr2O7	Li7Sn2
					1.031	-0.0509/-0.034	La2O3	Li2O	Li6Zr2O7	Li17Sn4
					7.281	-0.0508/-0.037	La2O3	Li2O	Zr3O	Li17Sn4
					7.594	-0.0507/-0.037	La2O3	Li2O	Zr4O	Li17Sn4
					8.531	-0.0491	La2O3	Li2O	Zr	Li17Sn4
Li56La24Zr15TeO96	Zr	Te	4	-3.090	0.750	-0.0687/-0.048	La2O3	Li2O	Li6Zr2O7	La2TeO2
					7.000	-0.0650/-0.048	La2O3	Li2O	Zr3O	La2TeO2
					7.312	-0.0647/-0.048	La2O3	Li2O	Zr4O	La2TeO2
					8.250	-0.0627	La2O3	Li2O	Zr	La2TeO2
Li56La24Zr15TiO96	Zr	Ti	4	-3.123	0.417	-0.0203/-0.002	La2O3	Li2O	Li6Zr2O7	Ti3O
					0.625	-0.0209/-0.003	La2O3	Li2O	Li6Zr2O7	ZrTi2O
					6.667	-0.0267/-0.012	La2O3	Li2O	Zr3O	ZrTi2O
					6.969	-0.0268/-0.012	La2O3	Li2O	Zr4O	ZrTi2O
					7.875	-0.0259	La2O3	Li2O	Zr	ZrTi2O
Li56La24Zr15IrO96	Zr	Ir	4	-3.082	0.500	-0.0603/-0.042	La2O3	Li2O	Li6Zr2O7	Ir
					0.667	-0.0649/-0.047	La2O3	Li2O	Li6Zr2O7	ZrIr3
					1.000	-0.0684/-0.050	La2O3	Li2O	Li6Zr2O7	ZrIr
					1.333	-0.0693/-0.051	La2O3	Li2O	Li6Zr2O7	Zr5Ir3
					2.000	-0.0692/-0.052	La2O3	Li2O	Li6Zr2O7	Zr3Ir
					7.000	-0.0662/-0.051	La2O3	Li2O	Zr3O	Zr3Ir
					7.250	-0.0660/-0.051	La2O3	Li2O	Zr4O	Zr3Ir
					8.000	-0.0643	La2O3	Li2O	Zr	Zr3Ir
Li56La24Zr15SeO96	Zr	Se	4	-3.085	0.667	-0.0705/-0.052	La2O3	Li2O	Li6Zr2O7	La4Se3O4
					0.750	-0.0759/-0.058	La2O3	Li2O	Li6Zr2O7	La2SeO2
					7.000	-0.0708/-0.056	La2O3	Li2O	Zr3O	La2SeO2
					7.312	-0.0705/-0.056	La2O3	Li2O	Zr4O	La2SeO2
					8.250	-0.0682	La2O3	Li2O	Zr	La2SeO2
Li56La24Zr15MnO96	Zr	Mn	4	-3.086	0.125	-0.0375/-0.009	La2O3	Li2O	Li6Zr2O7	LiMnO2
					0.250	-0.0457/-0.017	La2O3	Li2O	Li6Zr2O7	Li6MnO4
					0.500	-0.0563/-0.028	La2O3	Li2O	Li6Zr2O7	Mn
					0.750	-0.0576/-0.030	La2O3	Li2O	Li6Zr2O7	ZrMn2
					6.792	-0.0562/-0.034	La2O3	Li2O	Zr3O	ZrMn2
					7.094	-0.0560/-0.034	La2O3	Li2O	Zr4O	ZrMn2
					8.000	-0.0542	La2O3	Li2O	Zr	ZrMn2
Li56La24Zr15WO96	Zr	W	4	-3.094	0.500	-0.0485/-0.025	La2O3	Li2O	Li6Zr2O7	W
					0.750	-0.0494/-0.026	La2O3	Li2O	Li6Zr2O7	ZrW2

					6.792	-0.0496/-0.031	La2O3	Li2O	Zr3O	ZrW2
					7.094	-0.0495/-0.031	La2O3	Li2O	Zr4O	ZrW2
					8.000	-0.0479	La2O3	Li2O	Zr	ZrW2
Li56La24Zr15CoO96	Zr	Co	4	-3.082	0.125	-0.0344/-0.014	La2O3	Li2O	Li6Zr2O7	Li5CoO4
					0.250	-0.0438/-0.023	La2O3	Li2O	Li6Zr2O7	Li6CoO4
					0.500	-0.0603/-0.040	La2O3	Li2O	Li6Zr2O7	Co
					0.630	-0.0616/-0.041	La2O3	Li2O	Li6Zr2O7	Zr6Co23
					0.750	-0.0624/-0.042	La2O3	Li2O	Li6Zr2O7	ZrCo2
					1.000	-0.0627/-0.043	La2O3	Li2O	Li6Zr2O7	ZrCo
					1.500	-0.0633/-0.044	La2O3	Li2O	Li6Zr2O7	Zr2Co
					2.000	-0.0633/-0.044	La2O3	Li2O	Li6Zr2O7	Zr3Co
					7.000	-0.0612/-0.045	La2O3	Li2O	Zr3O	Zr3Co
					7.250	-0.0610/-0.045	La2O3	Li2O	Zr4O	Zr3Co
					8.000	-0.0594	La2O3	Li2O	Zr	Zr3Co
Li56La24Zr15CeO96	Zr	Ce	4	-3.163	0.045	0.0202/-0.002	La2O3	Li2O	Li6Zr2O7	Ce11O20
					0.050	0.0201/-0.002	La2O3	Li2O	Li6Zr2O7	Ce5O9
					0.071	0.0194/-0.003	La2O3	Li2O	Li6Zr2O7	Ce7O12
					0.125	0.0188/-0.004	La2O3	Li2O	Li6Zr2O7	Ce2O3
					0.250	0.0179/-0.004	La2O3	Li2O	Li6Zr2O7	CeO
					6.500	0.0039/-0.013	La2O3	Li2O	Zr3O	CeO
					6.812	0.0035/-0.014	La2O3	Li2O	Zr4O	CeO
					7.750	0.0035	La2O3	Li2O	Zr	CeO
Li56La24Zr15ThO96	Zr	Th	4	-3.167	0.500	0.0230	La2O3	Li2O	Li6Zr2O7	Th
					6.250	0.0005/-0.010	La2O3	Li2O	Zr3O	La2Th8O19
					6.562	0.0001/-0.010	La2O3	Li2O	Zr4O	La2Th8O19
					7.500	0.0003	La2O3	Li2O	Zr	La2Th8O19
Li56La24Zr15UO96	Zr	U	4	-3.158	0.500	0.0142/-0.005	La2O3	Li2O	Li6Zr2O7	U
					6.750	0.0010/-0.014	La2O3	Li2O	Zr3O	U
					7.062	0.0006/-0.014	La2O3	Li2O	Zr4O	U
					8.000	0.0008	La2O3	Li2O	Zr	U
Li56La24Zr15RuO96	Zr	Ru	4	-3.122	0.500	-0.0211/-0.038	La2O3	Li2O	Li6Zr2O7	Ru
					1.000	-0.0280/-0.044	La2O3	Li2O	Li6Zr2O7	ZrRu
					6.833	-0.0323/-0.045	La2O3	Li2O	Zr3O	ZrRu
					7.125	-0.0323/-0.045	La2O3	Li2O	Zr4O	ZrRu
					8.000	-0.0313	La2O3	Li2O	Zr	ZrRu
Li56La24Zr15TcO96	Zr	Tc	4	-3.127	0.500	-0.0162/-0.031	La2O3	Li2O	Li6Zr2O7	Tc
					0.750	-0.0189/-0.034	La2O3	Li2O	Li6Zr2O7	ZrTc2
					1.625	-0.0206/-0.035	La2O3	Li2O	Li6Zr2O7	LiZr2Tc
					7.042	-0.0258/-0.037	La2O3	Li2O	Zr3O	LiZr2Tc
					7.312	-0.0259/-0.037	La2O3	Li2O	Zr4O	LiZr2Tc
					8.125	-0.0251	La2O3	Li2O	Zr	LiZr2Tc

Li56La24Zr15ReO96	Zr	Re	4	-3.124	0.500	-0.0191/-0.027	La2O3	Li2O	Li6Zr2O7	Re
					0.604	-0.0206/-0.029	La2O3	Li2O	Li6Zr2O7	Zr5Re24
					0.750	-0.0221/-0.030	La2O3	Li2O	Li6Zr2O7	ZrRe2
					0.920	-0.0227/-0.031	La2O3	Li2O	Li6Zr2O7	Zr21Re25
					6.820	-0.0280/-0.034	La2O3	Li2O	Zr3O	Zr21Re25
					7.115	-0.0281/-0.034	La2O3	Li2O	Zr4O	Zr21Re25
					8.000	-0.0272	La2O3	Li2O	Zr	Zr21Re25
Li56La24Zr15OsO96	Zr	Os	4	-3.119	0.500	-0.0240/-0.037	La2O3	Li2O	Li6Zr2O7	Os
					0.750	-0.0272/-0.040	La2O3	Li2O	Li6Zr2O7	ZrOs2
					1.000	-0.0297/-0.042	La2O3	Li2O	Li6Zr2O7	ZrOs
					1.625	-0.0309/-0.043	La2O3	Li2O	Li6Zr2O7	LiZr2Os
					7.042	-0.0343/-0.044	La2O3	Li2O	Zr3O	LiZr2Os
					7.312	-0.0343/-0.044	La2O3	Li2O	Zr4O	LiZr2Os
					8.125	-0.0333	La2O3	Li2O	Zr	LiZr2Os
Li55La24Zr15AsO96	Zr	As	5	-3.138	0.625	-0.0215/-0.034	La2O3	Li2O	Li6Zr2O7	As
					0.750	-0.0264/-0.038	La2O3	Li2O	Li6Zr2O7	LiAs
					1.000	-0.0357/-0.048	La2O3	Li2O	Li6Zr2O7	Li3LaAs2
					2.125	-0.0371/-0.048	La2O3	Li2O	Li6Zr2O7	Zr3As
					7.125	-0.0393/-0.049	La2O3	Li2O	Zr3O	Zr3As
					7.375	-0.0393/-0.048	La2O3	Li2O	Zr4O	Zr3As
					8.125	-0.0382	La2O3	Li2O	Zr	Zr3As
Li55La24Zr15ClO96	Zr	Cl	5	-3.106	0.750	-0.0743/-0.085	La2O3	Li2O	Li6Zr2O7	LiCl
					7.000	-0.0695/-0.078	La2O3	Li2O	Zr3O	LiCl
					7.312	-0.0691/-0.077	La2O3	Li2O	Zr4O	LiCl
					8.250	-0.0669	La2O3	Li2O	Zr	LiCl
Li55La24Zr15IO96	Zr	I	5	-3.119	0.750	-0.0529/-0.064	La2O3	Li2O	Li6Zr2O7	LaIO
					7.000	-0.0524/-0.061	La2O3	Li2O	Zr3O	LaIO
					7.312	-0.0522/-0.061	La2O3	Li2O	Zr4O	LaIO
					8.250	-0.0505	La2O3	Li2O	Zr	LaIO
Li55La24Zr15NbO96	Zr	Nb	5	-3.165	0.250	0.0140/-0.006	La2O3	Li2O	Li6Zr2O7	LiNbO2
					0.625	0.0049/-0.015	La2O3	Li2O	Li6Zr2O7	Nb
					6.875	-0.0064/-0.022	La2O3	Li2O	Zr3O	Nb
					7.187	-0.0067/-0.022	La2O3	Li2O	Zr4O	Nb
					8.125	-0.0063	La2O3	Li2O	Zr	Nb
Li55La24Zr15SbO96	Zr	Sb	5	-3.144	0.625	-0.0156/-0.034	La2O3	Li2O	Li6Zr2O7	Sb
					0.875	-0.0245/-0.043	La2O3	Li2O	Li6Zr2O7	La2SbO2
					1.000	-0.0282/-0.047	La2O3	Li2O	Li6Zr2O7	Li3Sb
					7.250	-0.0327/-0.047	La2O3	Li2O	Zr3O	Li3Sb
					7.562	-0.0327/-0.047	La2O3	Li2O	Zr4O	Li3Sb
					8.500	-0.0316	La2O3	Li2O	Zr	Li3Sb
Li55La24Zr15VO96	Zr	V	5	-3.150	0.250	0.0030/-0.012	La2O3	Li2O	Li6Zr2O7	LiVO2

					0.625	-0.0098/-0.024	La2O3	Li2O	Li6Zr2O7	V
					6.875	-0.0181/-0.029	La2O3	Li2O	Zr3O	V
					7.187	-0.0183/-0.029	La2O3	Li2O	Zr4O	V
					8.125	-0.0175	La2O3	Li2O	Zr	V
Li55La24Zr15TaO96	Zr	Ta	5	-3.172	0.625	0.0117/-0.009	La2O3	Li2O	Li6Zr2O7	Ta
					6.875	-0.0009/-0.017	La2O3	Li2O	Zr3O	Ta
					7.187	-0.0013/-0.017	La2O3	Li2O	Zr4O	Ta
					8.125	-0.0010	La2O3	Li2O	Zr	Ta
Li55La24Zr15PaO96	Zr	Pa	5	-3.179	0.625	0.0186/-0.002	La2O3	Li2O	Li6Zr2O7	Pa
					6.875	0.0045/-0.011	La2O3	Li2O	Zr3O	Pa
					7.187	0.0041/-0.012	La2O3	Li2O	Zr4O	Pa
					8.125	0.0042	La2O3	Li2O	Zr	Pa
Li54La24Zr15TeO96	Zr	Te	6	-3.107	1.000	-0.0836/-0.064	La2O3	Li2O	Li6Zr2O7	La2TeO2
					7.25	-0.0769/-0.061	La2O3	Li2O	Zr3O	La2TeO2
					7.562	-0.0765/-0.061	La2O3	Li2O	Zr4O	La2TeO2
					8.500	-0.0741	La2O3	Li2O	Zr	La2TeO2
Li54La24Zr15MoO96	Zr	Mo	6	-3.118	0.750	-0.0568/-0.041	La2O3	Li2O	Li6Zr2O7	Mo
					1.000	-0.0576/-0.042	La2O3	Li2O	Li6Zr2O7	ZrMo2
					7.042	-0.0562/-0.043	La2O3	Li2O	Zr3O	ZrMo2
					7.344	-0.0560/-0.043	La2O3	Li2O	Zr4O	ZrMo2
					8.250	-0.0543	La2O3	Li2O	Zr	ZrMo2

Table S2. The calculated energy barrier of Li ions migration by BVSE method in ab plane and along c-axis in LLZO and LLZOM, respectively. If ignoring the difference of hopping lengths (a=1Å), and frequencies (ν=10^{13} Hz) in these structures, the estimated diffusion coefficient D will be obtained by the equation $D = \nu a^2 \exp(-E/k_BT)$ at 300K.[2, 3]

System	E_a (eV)	E_b(eV)	E_c(eV)	D_a(cm²/s)	D_b(cm²/s)	D_c(cm²/s)
$Li_7La_3Zr_2O_{12}$	0.94	0.95	0.94	1.62E-19	1.10E-19	1.62E-19
Fe2+(Zr)	1.06	1.05	1.05	1.56E-21	2.29E-21	2.29E-21
Be2+(Zr)	1.04	1.06	1.06	3.38E-21	1.56E-21	1.56E-21
Mg2+(Zr)	1.06	1.05	1.05	1.56E-21	2.29E-21	2.29E-21
Cd2+(Zr)	1.03	1.04	1.04	4.97E-21	3.38E-21	3.38E-21
Eu2+(Zr)	1.23	1.21	1.22	2.17E-24	4.71E-24	3.20E-24
Cu2+(Zr)	1.05	1.07	1.05	2.29E-21	1.06E-21	2.29E-21
Hg2+(Zr)	1.02	1.04	1.03	7.32E-21	3.38E-21	4.97E-21
Ni2+(Zr)	1.05	1.04	1.04	2.29E-21	3.38E-21	3.38E-21
Ca2+(Zr)	1.03	1.04	1.04	4.97E-21	3.38E-21	3.38E-21
Sr2+(Zr)	1	1.04	1.02	1.59E-20	3.38E-21	7.32E-21
Zn2+(Zr)	1.03	1.05	1.09	4.97E-21	2.29E-21	4.88E-22
Mn2+(Zr)	1.05	1.05	1.05	2.29E-21	2.29E-21	2.29E-21

Co2+(Zr)	1.04	1.07	1.04	3.38E-21	1.06E-21	3.38E-21
Cr3+(Zr)	0.93	0.91	0.91	2.38E-19	5.16E-19	5.16E-19
Rh3+(Zr)	0.94	0.92	0.92	1.62E-19	3.50E-19	3.50E-19
In3+(Zr)	0.94	0.91	0.91	1.62E-19	5.16E-19	5.16E-19
Tl3+(Zr)	0.93	0.92	0.92	2.38E-19	3.50E-19	3.50E-19
Au3+(Zr)	0.94	0.94	0.93	1.62E-19	1.62E-19	2.38E-19
Sc3+(Zr)	0.94	0.92	0.92	1.62E-19	3.50E-19	3.50E-19
Tm3+(Zr)	0.94	0.93	0.93	1.62E-19	2.38E-19	2.38E-19
Er3+(Zr)	0.94	0.92	0.92	1.62E-19	3.50E-19	3.50E-19
Ho3+(Zr)	0.94	0.93	0.93	1.62E-19	2.38E-19	2.38E-19
Sm3+(Zr)	0.94	0.92	0.92	1.62E-19	3.50E-19	3.50E-19
Y3+(Zr)	0.94	0.93	0.93	1.62E-19	2.38E-19	2.38E-19
Dy3+(Zr)	0.94	0.93	0.93	1.62E-19	2.38E-19	2.38E-19
Tb3+(Zr)	0.94	0.93	0.93	1.62E-19	2.38E-19	2.38E-19
Ce3+(Zr)	0.93	0.93	0.94	2.38E-19	2.38E-19	1.62E-19
Nd3+(Zr)	0.93	0.93	0.93	2.38E-19	2.38E-19	2.38E-19
Bi3+(Zr)	0.94	0.93	0.93	1.62E-19	2.38E-19	2.38E-19
Ga3+(Zr)	0.93	0.92	0.92	2.38E-19	3.50E-19	3.50E-19
Al3+(Zr)	0.91	0.91	0.9	5.16E-19	5.16E-19	7.60E-19
Fe3+(Zr)	0.94	0.92	0.92	1.62E-19	3.50E-19	3.50E-19
Ru3+(Zr)	0.93	0.92	0.92	2.38E-19	3.50E-19	3.50E-19
As3+(Zr)	0.92	0.94	0.92	3.50E-19	1.62E-19	3.50E-19
Co3+(Zr)	0.93	0.92	0.92	2.38E-19	3.50E-19	3.50E-19
P3+(Zr)	0.9	0.91	0.92	7.60E-19	5.16E-19	3.50E-19
Th4+(Zr)	0.93	0.93	0.95	2.38E-19	2.38E-19	1.10E-19
Ce4+(Zr)	0.93	0.93	0.93	2.38E-19	2.38E-19	2.38E-19
C4+(Zr)	0.93	0.93	0.91	2.38E-19	2.38E-19	5.16E-19
Si4+(Zr)	0.93	0.94	0.93	2.38E-19	1.62E-19	2.38E-19
Sn4+(Zr)	0.94	0.94	0.94	1.62E-19	1.62E-19	1.62E-19
Hf4+(Zr)	0.94	0.94	0.94	1.62E-19	1.62E-19	1.62E-19
Ti4+(Zr)	0.94	0.94	0.94	1.62E-19	1.62E-19	1.62E-19
Ge4+(Zr)	0.93	0.94	0.93	2.38E-19	1.62E-19	2.38E-19
Pb4+(Zr)	0.94	0.95	0.93	1.62E-19	1.10E-19	2.38E-19
Mo4+(Zr)	0.92	0.95	0.92	3.50E-19	1.10E-19	3.50E-19
Pt4+(Zr)	0.93	0.95	0.93	2.38E-19	1.10E-19	2.38E-19
Pd4+(Zr)	0.93	0.94	0.93	2.38E-19	1.62E-19	2.38E-19
W4+(Zr)	0.93	0.94	0.93	2.38E-19	1.62E-19	2.38E-19
Se4+(Zr)	0.93	0.96	0.93	2.38E-19	7.46E-20	2.38E-19
Ir4+(Zr)	0.93	0.94	0.93	2.38E-19	1.62E-19	2.38E-19
Te4+(Zr)	0.94	0.94	0.93	1.62E-19	1.62E-19	2.38E-19
Ru4+(Zr)	0.94	0.92	0.92	1.62E-19	3.50E-19	3.50E-19
Re4+(Zr)	0.93	0.93	0.92	2.38E-19	2.38E-19	3.50E-19
Os4+(Zr)	0.94	0.92	0.92	1.62E-19	3.50E-19	3.50E-19
S4+(Zr)	0.95	0.95	0.92	1.10E-19	1.10E-19	3.50E-19
Ta5+(Zr)	0.9	0.91	0.9	7.60E-19	5.16E-19	7.60E-19

Nb5+(Zr)	0.91	0.91	0.91	5.16E-19	5.16E-19	5.16E-19
V5+(Zr)	0.9	0.91	0.9	7.60E-19	5.16E-19	7.60E-19
As5+(Zr)	0.91	0.94	0.92	5.16E-19	1.62E-19	3.50E-19
Sb5+(Zr)	0.93	0.92	0.93	2.38E-19	3.50E-19	2.38E-19
I5+(Zr)	0.92	0.89	0.93	3.50E-19	1.12E-18	2.38E-19
Mo6+(Zr)	0.91	0.86	0.89	5.16E-19	3.57E-18	1.12E-18
Te6+(Zr)	0.88	0.88	0.88	1.65E-18	1.65E-18	1.65E-18
W6+(Zr)	0.92	0.93	0.92	3.50E-19	2.38E-19	3.50E-19
Na1+(La)	1.04	1.06	1.06	3.38E-21	1.56E-21	1.56E-21
K1+(La)	1.05	1.06	1.06	2.29E-21	1.56E-21	1.56E-21
Rb1+(La)	1.08	1.06	0.99	7.19E-22	1.56E-21	2.34E-20
Cs1+(La)	1.07	1.07	1.05	1.06E-21	1.06E-21	2.29E-21
Ag1+(La)	1.09	1.1	1.09	4.88E-22	3.32E-22	4.88E-22
Sr2+(La)	1.05	1.05	1.05	2.29E-21	2.29E-21	2.29E-21
Ba2+(La)	1.06	1.04	1.04	1.56E-21	3.38E-21	3.38E-21
Ca2+(La)	1.04	1.03	1.04	3.38E-21	4.97E-21	3.38E-21
Pb2+(La)	1.06	1.04	1.04	1.56E-21	3.38E-21	3.38E-21
Cd2+(La)	1.03	1.05	1.05	4.97E-21	2.29E-21	2.29E-21
Bi3+(La)	0.94	0.92	0.92	1.62E-19	3.50E-19	3.50E-19
Dy3+(La)	0.94	0.94	0.92	1.62E-19	1.62E-19	3.50E-19
Er3+(La)	0.94	0.94	0.93	1.62E-19	1.62E-19	2.38E-19
Ho3+(La)	0.94	0.94	0.93	1.62E-19	1.62E-19	2.38E-19
Lu3+(La)	0.93	0.93	0.92	2.38E-19	2.38E-19	3.50E-19
Nd3+(La)	0.94	0.94	0.91	1.62E-19	1.62E-19	5.16E-19
Pr3+(La)	0.94	0.94	0.92	1.62E-19	1.62E-19	3.50E-19
Sm3+(La)	0.93	0.93	0.91	2.38E-19	2.38E-19	5.16E-19
Tb3+(La)	0.94	0.94	0.92	1.62E-19	1.62E-19	3.50E-19
Y3+(La)	0.93	0.93	0.91	2.38E-19	2.38E-19	5.16E-19
Tm3+(La)	0.94	0.94	0.93	1.62E-19	1.62E-19	2.38E-19
Gd3+(La)	0.94	0.94	0.92	1.62E-19	1.62E-19	3.50E-19
Yb3+(La)	0.94	0.94	0.92	1.62E-19	1.62E-19	3.50E-19
Tl3+(La)	0.95	0.95	0.93	1.10E-19	1.10E-19	2.38E-19
Sc3+(La)	0.96	0.97	0.94	7.46E-20	5.07E-20	1.62E-19
Al3+(Li)	0.92	0.91	0.85	3.50E-19	5.16E-19	5.26E-18
Ga3+(Li)	0.94	0.92	0.87	1.62E-19	3.50E-19	2.42E-18
B3+(Li)	0.95	0.93	0.85	1.10E-19	2.38E-19	5.26E-18
Fe3+(Li)	0.94	0.92	0.85	1.62E-19	3.50E-19	5.26E-18
Cd2+(Li)	0.92	0.89	0.91	3.50E-19	1.12E-18	5.16E-19
Be2+(Li)	0.9	0.9	0.91	7.60E-19	7.60E-19	5.16E-19
Zn2+(Li)	0.9	0.9	0.9	7.60E-19	7.60E-19	7.60E-19
Co2+(Li)	0.92	0.9	0.91	3.50E-19	7.60E-19	5.16E-19
Mn2+(Li)	0.93	0.9	0.9	2.38E-19	7.60E-19	7.60E-19
Cu2+(Li)	0.92	0.9	0.91	3.50E-19	7.60E-19	5.16E-19
Pb4+(Li)	0.9	0.91	0.9	7.60E-19	5.16E-19	7.60E-19
Ti4+(Li)	0.94	0.91	0.95	1.62E-19	5.16E-19	1.10E-19

Table S3. The formation energies of the M_xO_y come from Materials Project Database.[1] The experimental formation energies[4, 5] as a feature is used by machine learning. Most of the formation energies are experimental values, only a few are calculated.

M_xO_y	$\Delta H_{f,x+y}$(eV/atom)		M_xO_y	$\Delta H_{f,x+y}$(eV/atom)		M_xO_y	$\Delta H_{f,x+y}$(eV/atom)	
System	Exp.	Cal.	System	Exp.	Cal.	System	Exp.	Cal.
MgO	-3.118	-3.065	Tb_2O_3	-3.866	-4.002	RuO_2	-1.054	-1.470
CdO	-1.342	-1.382	Tm_2O_3	-3.915	-4.108	TcO_2	-1.496	-1.900
EuO	-3.057	-3.136	Gd_2O_3	-3.813	-3.906	OsO_2	-1.019	-1.361
CuO	-0.807	-0.953	Yb_2O_3	-	-2.721	ReO_2	-1.523	-1.913
HgO	-0.471	-0.647	In_2O_3	-1.913	-2.013	UO_2	-3.748	-3.774
NiO	-1.242	-0.932	Sc_2O_3	-3.956	-3.984	SO_2	-	-1.759
CaO	-3.29	-3.312	Pu_2O_3	-3.462	-3.452	As_2O_3	-1.363	-1.641
MnO	-1.996	-2.000	Al_2O_3	-3.473	-3.442	CO_2	-	-1.783
FeO	-1.415	-1.679	Ga_2O_3	-2.261	-2.281	SO_2	-	-1.759
CoO	-1.233	-1.330	B_2O_3	-2.640	-2.813	Pa_2O_5	-	-2.742
SrO	-3.063	-3.093	Fe_2O_3	-1.71	-1.886	Ta_2O_5	-3.034	-3.355
BaO	-2.840	-2.835	P_2O_3	-	-1.972	Nb_2O_5	-2.812	-3.066
PbO	-1.133	-1.481	N_2O_3	-	-0.607	V_2O_5	-2.296	-2.316
BeO	-3.158	-3.115	Co_2O_3	-	-1.057	As_2O_5	-1.371	-1.576
ZnO	-1.816	-1.797	Am_2O_3	-3.504	-	Sb_2O_5	-1.439	-1.766
Cr_2O_3	-2.364	-2.350	ThO_2	-4.237	-4.387	I_2O_5	-	-0.772
Rh_2O_3	-0.737	-1.087	CeO_2	-3.767	-3.945	Cl_2O_5	-	-0.224
Tl_2O_3	-0.802	-1.120	SiO_2	-3.146	-3.285	Np_2O_5	-3.201	-3.447
Au_2O_3	-0.007	-0.466	SnO_2	-1.996	-2.125	MoO_3	-1.929	-2.023
Ce_2O_3	-3.731	-3.777	HfO_2	-3.854	-4.039	TeO_3	-	-1.359
Ir_2O_3	-	-0.958	TiO_2	-3.261	-3.519	UO_3	-3.171	-3.131
Ru_2O_3	-	-1.141	GeO_2	-2.003	-2.094	WO_3	-2.184	-2.178
Bi_2O_3	-	-1.654	PbO_2	-0.948	-1.317	Na_2O	-1.444	-1.454
Ac_2O_3	-	-3.752	MoO_2	-2.036	-2.150	K_2O	-1.250	-1.257
Dy_2O_3	-3.861	-4.027	PtO_2	-	-0.940	Rb_2O	-1.168	-1.118
Er_2O_3	-3.934	-4.074	PdO_2	-	-0.740	Cs_2O	-1.197	-1.197
Ho_2O_3	-3.899	-4.052	CoO_2	-	-1.138	Ag_2O	-0.108	-0.329
Lu_2O_3	-3.893	-4.139	MnO_2	-1.797	-1.811	Br_2O_3	-	-0.209
Nd_2O_3	-3.748	-3.799	WO_2	-2.038	-2.024	Sm_2O_3	-3.787	-3.879
Pm_2O_3	-3.752	-3.854	SeO_2	-0.779	-1.167	TeO_2	-1.122	-1.509
Pr_2O_3	-3.751	-3.750	IrO_2	-0.862	-1.260	Sb_2O_3	-1.469	-1.767

Table S4. Bond Dissociation Energies of M-O from handbook of Chemical Bond Energies.[6]

M-O	Bond Dissociation Energy(BDE)		M-O	Bond Dissociation Energy(BDE)	
	KJ/mol	eV		KJ/mol	eV
Mg-O	358.2	3.71	Ti-O	666.5	6.91
Cd-O	236	2.45	Ge-O	657.5	6.81
Eu-O	473	4.90	Pb-O	382.4	3.96
Cu-O	287.4	2.98	Mo-O	502	5.20
Hg-O	269	2.79	Pt-O	418.6	4.34
Ni-O	366	3.79	Pd-O	238.1	2.47
Ca-O	383.3	3.97	W-O	720	7.46
Sr-O	426.3	4.42	Se-O	429.7	4.45
Zn-O	250	2.59	Te-O	377	3.91
Mn-O	362	3.75	Tc-O	548	5.68
Co-O	397.4	4.12	Re-O	627	6.50
Cr-O	461	4.78	Os-O	575	5.96
Rh-O	405	4.20	Pa-O	792	8.21
In-O	346	3.59	Ta-O	839	8.70
Tl-O	213	2.21	Nb-O	726.5	7.53
Au-O	223	2.31	V-O	637	6.60
Sc-O	671.4	6.96	As-O	484	5.02
Tm-O	514	5.33	Sb-O	434	4.50
Er-O	606	6.28	I-O	233.4	2.42
Ho-O	606	6.28	Cl-O	267.47	2.77
Y-O	714.1	7.40	Be-O	437	4.53
Dy-O	615	6.37	Nd-O	703	7.29
Tb-O	694	7.19	Sm-O	573	5.94
Ce-O	790	8.19	Na-O	270	2.80
Pm-O	674	6.99	K-O	271.5	2.81
Bi-O	337.2	3.49	Rb-O	276	2.86
Ga-O	374	3.88	Cs-O	293	3.04
Al-O	501.9	5.20	Ag-O	221	2.29
Ir-O	414	4.29	Ba-O	562	5.82
Fe-O	407	4.22	Ac-O	794	8.23
Ru-O	528	5.47	Lu-O	669	6.93
P-O	589	6.10	Pr-O	740	7.67
Th-O	877	9.09	Y-O	714.1	7.40
Sn-O	528	5.47	Yb-O	387.7	4.02
Hf-O	801	8.30	Be-O	437	4.53

Table S5. A summary of top-5 models with two feature pair in the SVM algorithm.[7] For each feature pair, we used five-fold cross-validation on a 0.8/0.2 training/testing split of the dataset. In (score±error), score and error are calculated as the mean score. Accuracy is calculated as the fraction of correctly predicted materials as stable or unstable. Precision is defined as the fraction of predicted stable compounds that are actually stable, and recall is defined as the fraction of actual stable compounds that are predicted stable. The F_1 score is a metric that incorporates both precision and recall.

Feature pair	Accuracy	Precision	Recall	F_1 score
($\Delta H_{f,x+y}$, CN*$\Delta H_{f,x}$)	0.99(±0.02)	0.98(±0.03)	0.99(±0.01)	0.99(±0.02)
($\Delta H_{f,x+y}$, BDE)	0.98(±0.04)	0.97(±0.06)	0.99(±0.02)	0.98(±0.05)
($\Delta H_{f,x+y}$, χ_M)	0.98(±0.02)	0.97(±0.04)	0.99(±0.02)	0.98(±0.03)
($\Delta H_{f,x+y}$, CN*$\Delta H_{f,y}$)	0.97(±0.02)	0.95(±0.04)	0.98(±0.02)	0.96(±0.03)
($\Delta H_{f,x+y}$, 1st IE_M)	0.97(±0.04)	0.95(±0.06)	0.98(±0.03)	0.95(±0.05)

Table S6. Model predicted 18 LLZOM systems with relevant statistics, label 1 and -1 are thermodynamically stable and unstable, respectively. Seven of the systems were verified by DFT calculation.

System	*MxOy*	$\Delta H_{f,x+y}$ (eV/atom)	χ_M	Predicted ΔG (eV/f.u.)	Calculated ΔG (eV/f.u.)	Reaction products
Pm^{3+}(Zr)	Pm_2O_3	-3.752	1.13	0.322	0.183	Li2O3, Li2O, Zr4O, Pm2O3
Pm^{3+}(La)	Pm_2O_3	-3.752	1.13	0.247	0.198	Li2O3, Li2O, Zr4O, Pm2O3
U^{4+}(Zr)	UO_2	-3.748	1.38	0.189	0.020	Li2O3, Li2O, Zr4O, U
Th^{4+}(Zr)	ThO_2	-4.237	1.32	0.250	0.004	Li2O3, Li2O, Zr4O, La2Th8O19
Ac^{3+}(La)	Ac_2O_3	-3.580	1.09	0.169	0.230	Li2O3, Li2O, Zr4O, Ac2O3
Ce^{3+}(La)	Ce_2O_3	-3.731	1.12	0.257	0.155	Li2O3, Li2O, Zr4O, CeO
Sc^{3+}(La)	Sc_2O_3	-3.956	1.36	0.016	-0.008	Li2O3, Li2O, Zr4O, LiScO2
W^{6+}(Zr)	WO_3	-2.184	2.12	-0.456	-0.802	Li2O3, Li2O, Zr4O, ZrW2
As^{3+}(Zr)	As_2O_3	-1.363	2.18	-0.377	-0.725	Li2O3, Li2O, Zr4O, Zr3As
Co^{3+}(Zr)	Co_2O_3	-1.057	1.88	-0.213	-0.626	Li2O3, Li2O, Zr4O, Zr3Co
Pa^{5+}(Zr)	Pa_2O_5	-2.692	1.54	-0.352	0.127	Li2O3, Li2O, Zr4O, Pa
Co^{2+}(Li)	CoO	-1.233	1.88	-0.212	-0.527	Li2O3, Li2O, Zr4O, Zr3Co
Mn^{2+}(Li)	MnO	-1.996	1.55	-0.216	-0.553	Li2O3, Li2O, Zr4O, ZrMn2
Fe^{2+}(Li)	FeO	-1.415	1.83	-0.216	-0.318	Li2O3, Li2O, Zr4O, Zr3Fe

Mg^{2+}(Li)	MgO	-3.118	1.31	-0.232	-0.086	Li2O3, Li2O, Zr4O, Li5Mg
Cu^{2+}(Li)	CuO	-0.807	1.90	-0.212	-0.568	Li2O3, Li2O, Zr4O, Zr2Cu
Pb^{4+}(Li)	PbO_2	-0.948	1.87	-0.265	-0.564	Li2O3, Li2O, Zr4O, Li17Pb4
Ti^{4+}(Li)	TiO_2	-3.261	1.54	-0.215	-0.066	Li2O3, Li2O, Zr4O, ZrTi2O

Table S7. The structures and band gaps for the list of compounds come from the Materials Project.[1]

Material_Id	**Formula**	**Spacegroup**	**Band Gap (eV)**
mp-2605	CaO	Fmm	3.634
mp-1216	YbO	Fmm	3.460
mp-772185	$Li_6Hf_2O_7$	C2/c	4.413
mp-976280	LiBr	$P6_3mc$	4.935
mp-1185319	LiCl	$P6_3mc$	5.928
mp-4547	La_2TeO_2	I4/mmm	2.029
mp-7233	La_2SeO_2	Pm1	2.407
mp-4511	La_2SO_2	Pm1	3.061
mp-30993	LaIO	P4/nmm	3.289
mp-2292	La_2O_3	Ia	3.532
mp-1960	Li_2O	Fmm	4.899
mp-5418	$Li_6Zr_2O_7$	C2/c	3.944

Table S8 Comparison of mean squared error (MSE) and coefficient of determination (R^2) between five regression models for prediction of reaction energy.

Model	**Linear Regression**	**Gradient Boosting**	**Decision tree Regression**	**Kernel Ridge Regression**	**Random Forest**
MSE	0.15	0.10	0.09	0.04	0.06
R^2	0.69	0.80	0.82	0.92	0.90

(a)

Stability of Dopants in $Li_7La_3Zr_2O_{12}$

Li site
La site
Zr site

IA	IIA							VIII			IB	IIB	IIIA	IVA	VA	VIA	VIIA
Li	Be (2+)												B (3+)	C (4+)	N (3+)	O	F
Na (1+)	Mg (2+)	IIIB	IVB	VB	VIB	VIIB							Al (3+)	Si (4+)	P (3+)	S (4+)	Cl (5+)
K (1+)	Ca (2+)	Sc (3+)	Ti (4+)	V (5+)	Cr (3+)	Mn (4+)	Fe (3+)	Co (4+)	Ni (2+)	Cu (2+)	Zn (2+)		Ga (3+)	Ge (4+)	As (5+)	Se (4+)	Br (3+)
Rb (1+)	Sr (2+)	Y (3+)	Zr	Nb (5+)	Mo(4+)	Tc (4+)	Ru (4+)	Rh (3+)	Pd (4+)	Ag (1+)	Cd (2+)		In (3+)	Sn (4+)	Sb (5+)	Te (4+)	I (5+)
Cs (1+)	Ba (2+)	La-Lu	Hf (4+)	Ta (5+)	W (4+)	Re(4+)	Os(4+)	Ir (4+)	Pt (4+)	Au (3+)	Hg (2+)		Tl (3+)	Pb (4+)	Bi (3+)	Po	At
Fr	Ra	Ac-Lr	Rf	Db	Sg	Bh	Hs	Mt	Ds	Rg	Uub						

La-Lu	La	Ce (4+)	Pr (3+)	Nd (3+)	Pm (3+)	Sm (3+)	Eu (2+)	Gd (3+)	Tb (3+)	Dy (3+)	Ho (3+)	Er (3+)	Tm (3+)	Yb(3+)	Lu (3+)
Ac-Lr	Ac (3+)	Th (4+)	Pa (5+)	U	Np	Pu	Am	Cm	Bk	Cf	Es	Fm	Md	No	Lr

(b)

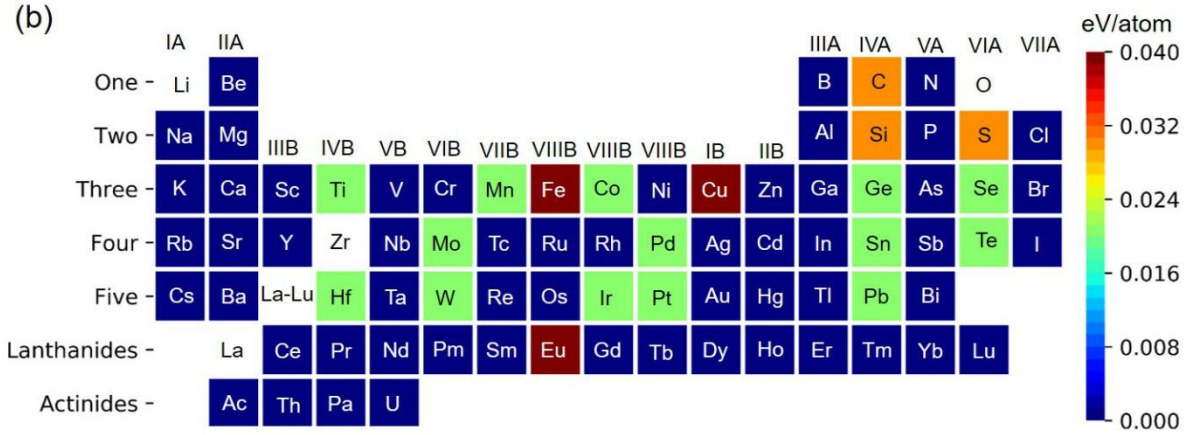

Figure S1. (a) Site and oxidation state preference for the dopant elements in LLZO and (b) calculated their energy above the convex hull.

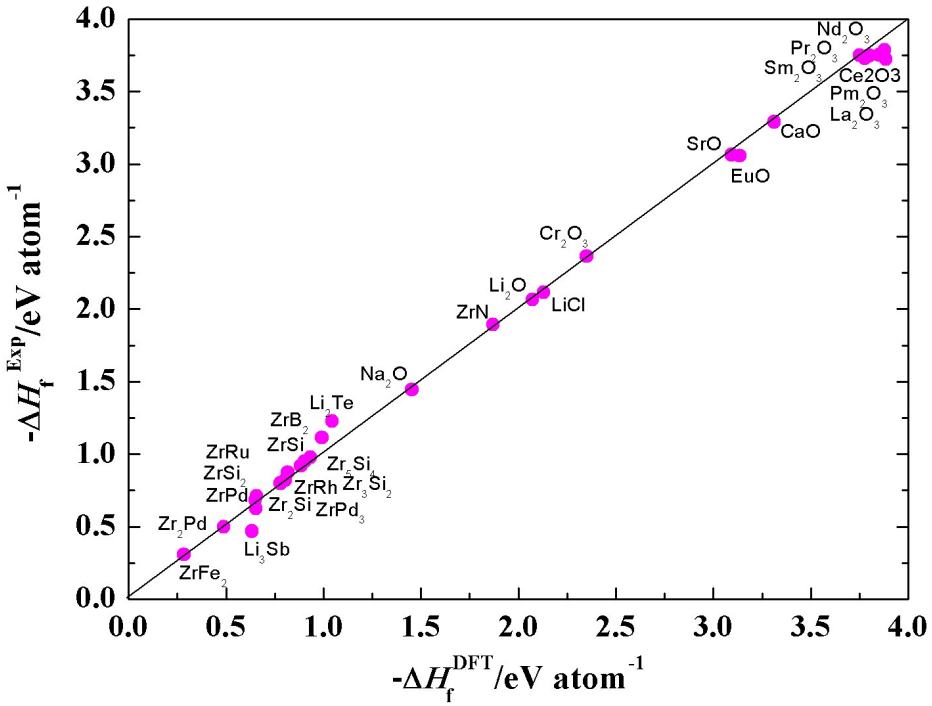

Figure S2. Comparison of the formation energies of some product phases calculated by DFT with the experimental values calculated using available thermodynamic database[4, 5].

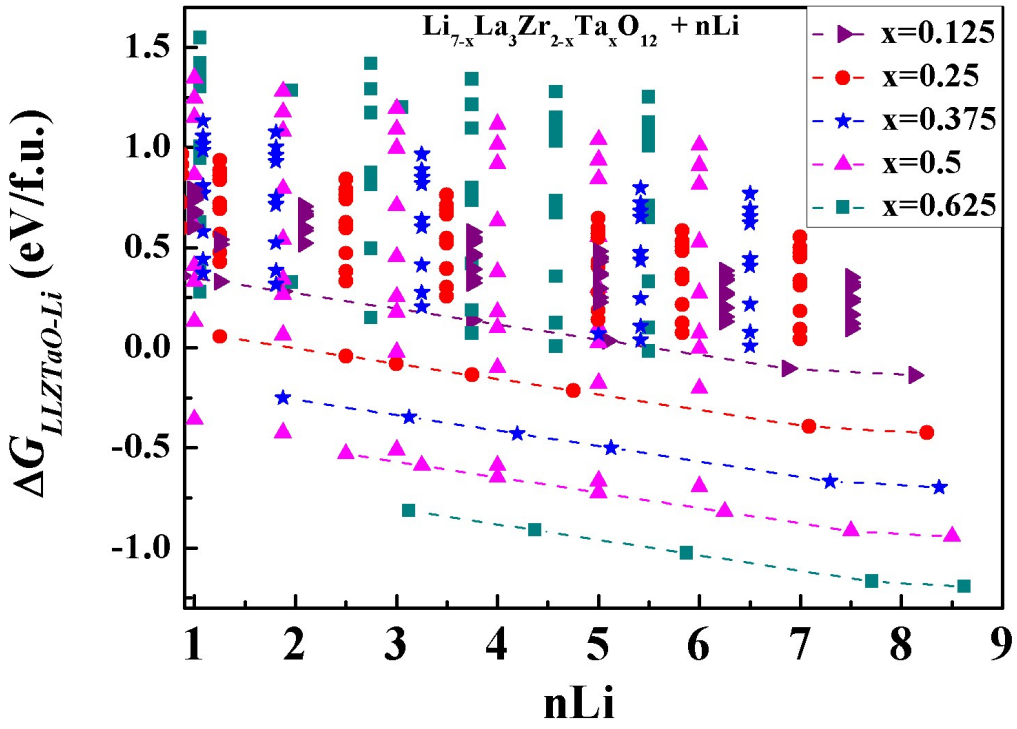

Figure S3. All possible reactions from the automatic reacting screening of $Li_{7-x}La_3Zr_{2-x}Ta_xO_{12}$ (x=0.125, 0.25, 0.375, 0.5, and 0.625) in contacting with different Li concentration (n Li).

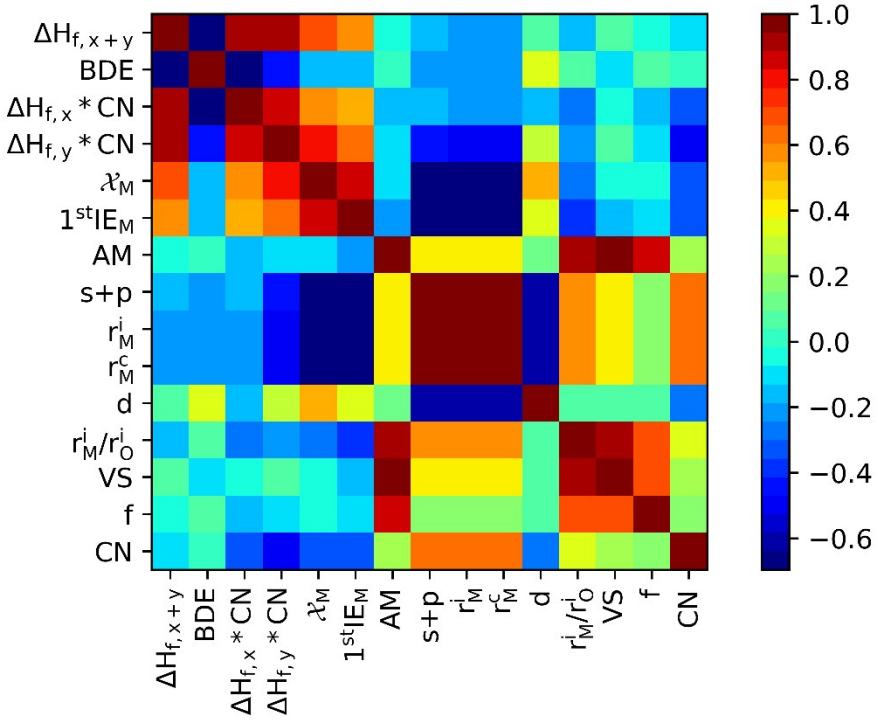

Figure S4. The heat map of Pearson correlation coefficient matrix among the features for LLZOM.

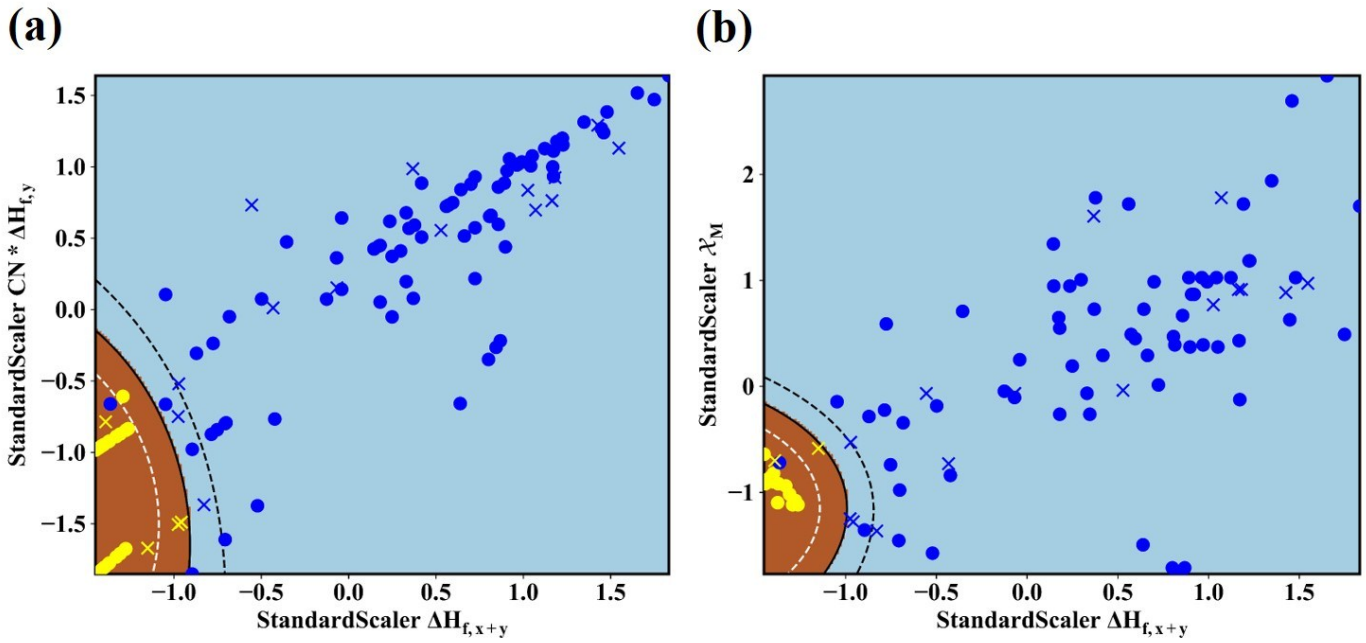

Figure S5. Maps of (a) $\Delta H_{f,x+y}$ and CN*$\Delta H_{f,y}$, (b) $\Delta H_{f,x+y}$ and Pauling electronegativity χ_M feature pairs.

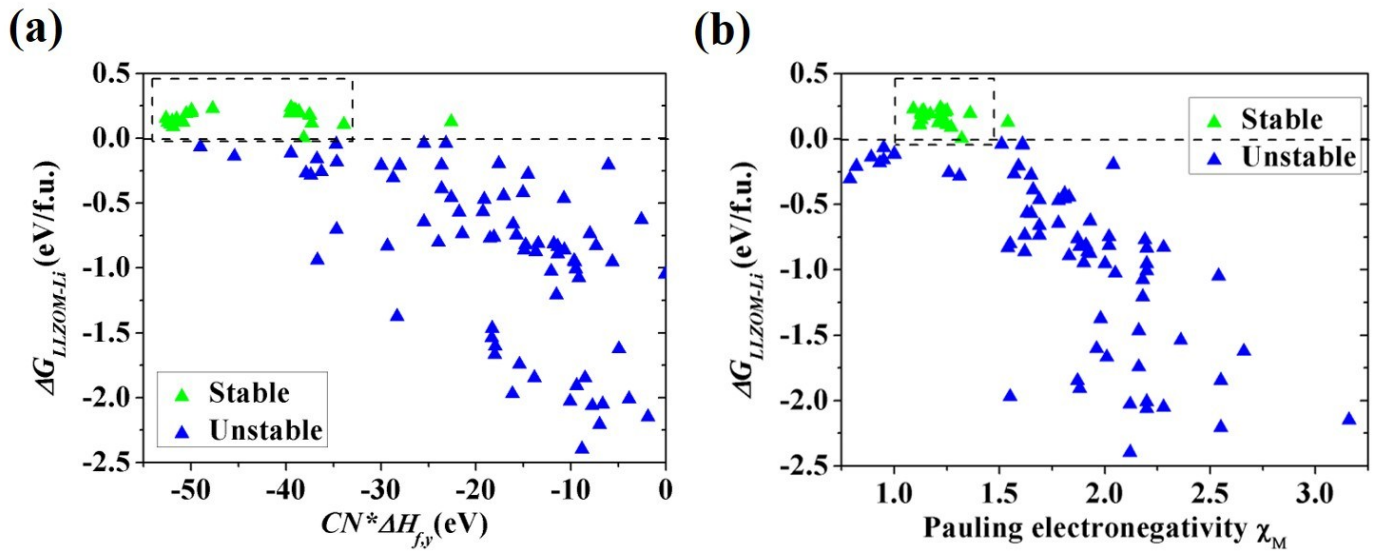

Figure S6. The reaction energy $\Delta G_{LLZOM\text{-}Li}$ of the Li|LLZOM interface dependence on (a) CN*$\Delta H_{f,y}$, and (b) Pauling electronegativity χ_M. The dotted boxes represent the most appropriate ranges for each feature.

References

1. S. P. Ong, W. D. Richards, A. Jain, G. Hautier, M. Kocher, S. Cholia, D. Gunter, V. L. Chevrier, K. A. Persson and G. Ceder, *Computational Materials Science*, 2013, **68**, 314-319.
2. G. H. Vineyard, *Journal of Physics and Chemistry of Solids*, 1957, **3**, 121-127.
3. B. Andriyevsky, K. Doll and T. Jacob, *Materials Chemistry and Physics*, 2017, **185**, 210-217.
4. P. Nash, *https://tptc.iit.edu/index.php/thermo-database*, 2013.

5. *Thermodynamic Properties of Inorganic Materials*, (Springer-Verlag:Berlin, Heidelberg, 1999), **Vol. 19**.
6. Y. R. Luo, *CRC Press, Boca Raton, FL*, 2007.
7. F. Pedregosa, Ga, #235, l. Varoquaux, A. Gramfort, V. Michel, B. Thirion, O. Grisel, M. Blondel, P. Prettenhofer, R. Weiss, V. Dubourg, J. Vanderplas, A. Passos, D. Cournapeau, M. Brucher, M. Perrot, #201 and d. Duchesnay, *J. Mach. Learn. Res.*, 2011, **12**, 2825-2830.